THIN FILM TEMPERATURE MEASUREMENTS

Lorenzo Battisti and Enrico Bertolazzi

Dip. Ingegneria Meccanica e Strutturale, Università di Trento,

via Mesiano 77, I – 38050 Trento, Italy

Fax : +39 0461 882599   Voice : +39 0461 882660

Abstract

Thin film based sensor in transient facility permits theoretically to perform very accurate surface temperature measurement, either because the low intrusivity of the gauge and the high frequency response. The mayor drawback for its popular use is the complexity of data reduction procedure which involves the solution of the heat conduction in solids. Among different techniques available, numerical discretization are gaining in importance for several applications basically because of their flexibility in treating boundary conditions and the low computational cost compared to other methods. After a brief analysis of the heat transfer evaluation criteria and the description of the sensor, a survey of the existing digital data processing technique are discussed in the first part of this paper, and some estimate of the accuracy is presented. The general case of multi-layered geometries of the sensor is analyzed and synthetic expression for the single and double layer features are given. Among the traditional methods, emphasis was placed on 1-D Finite Elements discretization, and a code has been developed to handle general heat transfer data reduction with arbitrary temperature or heat flux boundary conditions. Temperature dependent physical properties are also implemented. Validation of such a code has been performed by mens known test functions. Finally several experimental signal having different characteristics have been processed and the solution of the various methods compared and discussed.

Key words: Thin film, heat transfer, surface temperature measurements, Laplace Transform, Finite Elements.

1 Nomenclature

$\rho(z)$	one dimensional mass density of the slab;	$[kg/m^3]$
$c(z)$	the heat capacity of the slab;	$[J/kg \cdot K]$
$\kappa(z)$	the heat conduction of the slab;	$[W/m \cdot K]$
$\alpha = \kappa/\rho c$	thermal diffusivity;	$[m^2/s]$
δ	metal film thickness;	$[m]$
ℓ	total size of the slab;	$[m]$
$\dot{q}_s(t)$	impinging convective heat flux rate	$[W/m^2]$
$\dot{q}_b(t)$	back face convective heat flux rate	$[W/m^2]$
$u(t)$	internal density energy stored into the slab	$[J/m^2]$
$\Theta(t, z)$	temperature distribution of the slab	$[K]$
$\Theta^s(t)$	measured top surface temperature of the slab	$[K]$
$\Theta^\ell(t)$	measured bottom surface temperature of the slab	$[K]$
$\Theta^\infty(t)$	free stream temperature	$[K]$
$\mathrm{F}_c\,(t)$	Fresnel cosine function	
$\mathrm{F}_s\,(t)$	Fresnel sine function	
DAS	Digital Analog System	
ODE	Ordinary Differential Equation	
PDE	Partial Differential Equation	

2 Introduction

The evaluation of the heat flux rate impinging on a surface is an important task in engineering problems. Depending on the knowledge of the physical process involved the existing approaches can be grouped as follows:

(a) *Fully analytical approach*: this assumes a complete knowledge of the physical process involved. The heat flux is obtained by solving simultaneously the fully Navier-Stokes equations, the energy equation, the diffusion equation in solids, and the constitutive equations of the fluid and the body.

(b) *Experimental approach coupled with dimensional analysis*: the heat flux rate is evaluated through direct measurement of physically measurable quantities such as the boundary layer temperature distribution or the temperature distribution within the body.

(c) *Indirect method:* it prescribes the measurement of some physical quantities such as the body surface temperature. The heat flux rate is deduced by the solution of some auxiliary equations.

Approach (a) although very informative is still in most cases not reliable due to the complexity of 3-D turbulent modeling of the flow field. In fact also in the simpler 2-D cases large computational resources are needed. Actually, it is applicable for laminar flows only and for simple geometries. For example simplified equations describing velocities and boundary layer temperature distribution are available for the plane surface or for the cylinder in cross flow.

Approaches (b) and (c) require some data reduction procedure to compute the heat by analytical or numerical techniques. In particular, approach (b) calls for high performance hardware and, a part of the inherent relatively high costs, often it does not result technically feasible. Obviously approach (c) does not give any information for the comprehension of the transport phenomena. Yet, it has been in the years the most widely adopted because it requires limited number of measurements and involves only the solution of the diffusion equation in a body.

Short duration facilities have been preferred to the stationary ones for indirect methods because of the competitive running costs and the good accuracy measurement achievable. In fact the models have not to be cooled (or heated) in order to establish the temperature gradient from which the heat transfer is deduced. Consequently tests durations are shorter and the initial conditions are quickly restored. In net heat flux evaluation, conductive heat losses are not crucial. The measurement technique involves the measurement of the surface temperature history of a model exposed to a gas flow (supersonic or sub-sonic) on the basis of an appropriate heat conduction model.

Despite of the complexity of the data reduction procedure, a variety of techniques have been implemented and refined according to the type of test and sensor being used. A basic reference text describing measurement principles and data reduction techniques can be found in the work of Schultz and Jones (1973).

One of the most common fast response sensors for short duration test is the thin film resistance thermometer. A large body of literature is available on thin film heat transfer gauge. Diller (1991) gives an excellent survey of the related measurement technique. Here just a brief path of the progress in data reduction procedure will be drawn. Details of the sensors will be given in section 3.

The thin film surface temperature sensor has originally appeared in the early 1950s for heat transfer measurements in shock tubes. This facility can be operated to simulate either supersonic or sub-sonic environment depending on the locations of the throat respect to the working section. A very wide range of temperatures, from $500K$ to $2000K$ can be achieved. Depending on the hardware, typical test durations can range from $3ms$ (the Oxford shock tunnel) to a few seconds. A review is given in Vidal (1956), Pope & Goin (1965), Lukasiewicz (1973). Direct solution of the 1-D diffusion equation was initially performed by means of the electric analogy

(Meyer; 1960). In the 1960's some numerical integration techniques for the solution of the heat diffusion equation was proposed. All these schemes were based on approximate solution of the associate Laplace transform. The most popular one, proposed by Cook and Felderman (1966) will be addressed in section 5 and 6.

Starting from 1975 M.G. Dunn and its group in Calspan applied the thin film in order to measure heat flux distribution for gas turbine components. Vane row and full stage rotating turbine data have been subject of several papers Dunn and Hause (1981), Dunn et al. (1986), Dunn (1989). The progress in the computational media has made possible to improve the numerical techniques. The computer implementation of Fourier and Laplace transforms permitted to optimize the frequency response and the accuracy of the time-resolved results.

Wide experience on so called "double layer" thin films has been developed from the group working at the Oxford University initially under the direction of the late D.L. Schultz and with T.V. Jones, M.L.G. Oldfield, and R.W. Ainsworth.

The attempts to measure the mean heat transfer rate on real gas turbine components has lead to films instrumented on flexible electrically insulator substrate (kapton® or upilex®) to extend the use of this measurement technique to rotating test rig components where flow durations are of the order of a few seconds.

Analogue signal analysis has been used for data reduction on films built also with vitreous enamel substrate considering that the high frequency heat conduction in the insulating layer can for short times be considered as semi-infinite. An additional digital processing is moreover needed for the low frequency signal of the substrate layer Ainsworth et al. (1989), Doorly and Oldfield (1987), Doorly (1987), Guo et al. (1995).

At the von Karman Institute single layer thin film using mainly macor® as substrate has now been used for many years on the Mach 6 H-3 blow down wind tunnel, the long shot intermittent wind tunnel, and the CT 3 light piston facility. Recently double layer thin film with kapton® as substrate has been tested on low speed tunnels simulating flow conditions in gas turbine blade internal cooling channels. Main results can be found in Consigny and Richards (1982), Camci and Arts (1985), Arts and Bourguignon (1989), Battisti and Arts (1996) and Pelle and Arts (1997), Vermeulen and Simeonides (1992), Marquet and Charbonnier (1998).

The extension of the use of thin films to the evaluation of the fluctuating component of the heat transfer and the necessity to account for variable properties of the substrate has lead to a progressive phase out of the analogue technique.

Numerical techniques seemed to have the potential to provide for a powerful solving tool, up to now some data processing analysis were principally based on transforms such as Laplace or Fourier .

Both analogue and numerical transform based solution methods do present some limitation which basically are:

(i) the analog hardware necessitates a bandwidth depending on the sampling rate. An high sampling rate needs an hardware with very high bandwidth.

(ii) the impossibility to model variable thermal properties of the substrate(s) with the temperature;

(iii) operations are bounded to seminfinite slab assumption;

(iv) solution is computationally expensive with two substrate slab and, when the number of substrate slab excesses two, it becomes mathematically difficult to handle.

The best implementation of the aforementioned numerical techniques has complexity growing at least with $\mathcal{O}(n_s \log n_s)$ where n_s is the number of samples. Only approach (c) is analyzed and discussed in this paper. In the first part some data reduction techniques are reviewed. In the second part a general approach based on the Finite Elements is presented for fast and efficient heat flux computation. An economic and robust way is also given to estimate the convective heat transfer coefficient h which can be defined as (see fig. 1):

$$h \stackrel{def}{\equiv} \frac{\dot{q}_s(t)}{\Theta^\infty(t) - \Theta^s(t)} \tag{1}$$

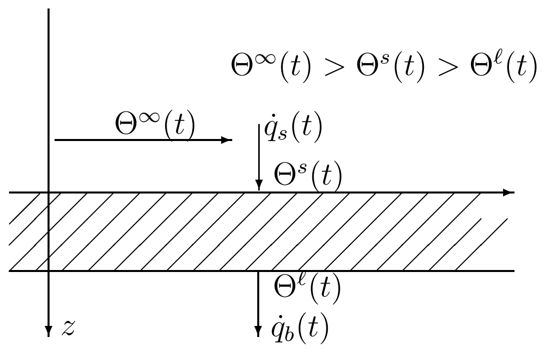

Fig. 1.

In formula (1) the free stream temperature $\Theta^\infty(t)$ and the surface temperature $\Theta^s(t)$ are known from standard measurement devices. The impinging heat flux rate $\dot{q}_s(t)$ can be inferred by an appropriate differential model of the substrate.

It is worth to remind that temperature $\Theta^s(t)$ is the result of a thermal balance among different heat fluxes. The principal ones are the convective heat flux $\dot{q}_s(t)$, the radiative heat flux, the conductive heat flux and heat flux due to electrical heat generation of measurements apparatus. In the following discussion it is assumed that the temperature $\Theta^s(t)$ depends only on the convective heat flux and the conductive heat flux, neglecting the others sources.

For a proper reconstruction of the signal an appropriate sampling rate must be assured. The limitation in the capacity of the acquisition system sets the maximal test duration. However the sampled data is usually huge and the postprocess is very time consuming if a transform based data reduction system is used. The Finite Elements based data reduction, proposed in this paper, is very fast, more flexible but, depending on the sampling rate, requires the correct setting of the mesh.

The proposed numerical scheme has been validated by using known exact solution of particular test cases, and by comparison with the classical numerical techniques.

A processing of three real signals is indeed given. The heat flux rate is deduced from surface temperature histories sampled on models running on different facilities. The first signal has been obtained from tests performed with a double layer thin films made by the University of Trento in low enthalpy and low speed test (about $\dot{q} = 1000W/m^2$, Re $= 30000$, Ma $= 0.02$) Battisti and Schmeer (1997). The second one is a signal sampled in the von Karman Institute CT1 tunnel at Mach number around 0.7 (single layer thin film). The last case has been obtained from a compression ramp in the H3 Mach 6 wind tunnel of the von Karman Institute (single layer thin film) Marquet and Charbonnier (1998).

The performance of the different solution schemes have been compared and commented.

3 The thin film surface temperature sensor

There are many different techniques currently available for surface temperatures measurement. The present paper is focused on the thin film resistance thermometer.

Basically the thin film gauge consists in a very thin conducting metal (platinum or nickel) deposited on homogeneous or disomogeneous substrate. As the metal acts as temperature sensor, the substrate serves either as mechanical support and as thermal heat sink. The most popular features of such devices are the single and the double layer thin film. The thermal behavior of these two kind of sensors will be analyzed forward.

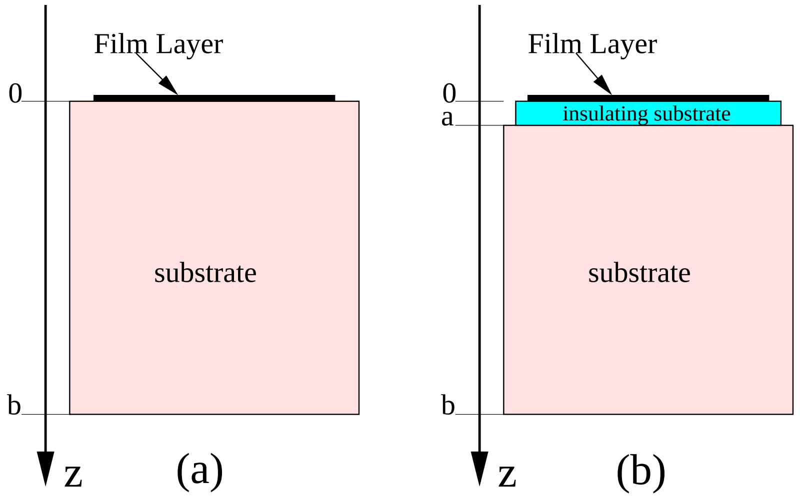

Fig. 2.

In the first type (see fig. 2a) the metal layer is fired or deposited on a substrate made of quartz or pyrex® or macor®. In particular the use of macor® (machinable) enables the desired shape model to be built without surface discontinuities. This makes the gauge particularly suitable for aerodynamic applications where the integrity of the boundary layer has to be preserved.

Such solutions are suitable for stationary components due to the limited deformation of the substrate. The double layer thin film (see fig. 2b) has been developed for measurement on rotating components. A thin insulating layer insulates electrically the metal film from the (metal) support. Either vitreous enamel is applied as insulating coating and plastic layer (kapton® or upilex®) adhesively bounded to the substrate.

A know constant current is passed through the gauge and the voltage drop across the film is directly related to the temperature of the gauge. When subjected to a change in the temperature field, the film acts as a thermometer and under some assumptions it shows the temperature evolution of the substrate surface. Since the typical thickness of the film ranges from $10^{-6}m$ to $10^{-8}m$ and this dimension is 10^5 times smaller than its typical length or width, the lateral conduction can be neglected. Therefore the one-dimensional heat conduction can generally be applied.

The characteristic time $\tau = \delta^2/\alpha$ of the film is dramatically small compared to the inner substrate one.

For the typical thickness given above, characteristic times range from $1.6 \cdot 10^{-3}\mu s$ (platinum painted on macor®) to $2 \cdot 10^{-4}s$ (nickel over kapton®). For a step function in surface heat transfer rate, the approximate solution for the relative error in the heat transfer rate computation:

$$t_H = \frac{q - \dot{q}_s}{\dot{q}_s},$$

as shown in Schultz and Jones 1977 can be estimated as follows for large t compared to τ:

$$t_H = \frac{1}{t^{1/2}} \frac{\tau^{1/2}}{\pi^{1/2}} \frac{((\rho c \kappa)_1)^{1/2}}{((\rho c \kappa)_2)^{1/2}}, \tag{2}$$

where the index 1 refers to the sensor and 2 to the supporting substrate. Relation (2) shows that error due the neglection of sensor presence drops as time increases. When maximum allowable error is given, relation (2) introduces a critical time in the initial part of the experiment. For $t_H \approx 10^{-2}$, this minimal duration takes the values of about $400\mu s$ for a typical double layer sensor to about $100\mu s$ for a single layer. The reciprocal of this critical time represents the critical frequency over over which the phenomenon is not accurately reconstructed.

The effect of the finite thickness of the sensible layer on the insulating substrate is thus to cause the actual surface temperature to lag the “real” one.

For general applications, other than shock tubes the presence of the film layer can be neglected if the experiment design is carefully set.

Whatever model being used, the heat flux rate can be generally evaluated from considerations about the transient thermal conduction in an inhomogeneous multi-slab substrate.

The governing equations for a general multi-slab substrate are addressed in the next section.

4 Governing equations

The 1-D diffusion equations for the temperature distribution of an $m-$layer slab having total size ℓ (see figure 3), can be modeled by the following m partial differential equations of parabolic type:

$$\frac{\partial}{\partial t}\left(\rho_i(\Theta_i)c_i(\Theta_i)\Theta_i\right) = \frac{\partial}{\partial z}\left(\kappa_i(\Theta_i)\frac{\partial \Theta_i}{\partial z}\right), \quad t>0, \quad z_{i-1}<z<z_i \quad i=1,2,\ldots,m \tag{3}$$

where $\Theta_i \equiv \Theta_i(t,z)$ and z_i are the boundaries of the layers. Equations (3) are coupled with the following $m-1$ interface conditions:

$$\left.\begin{aligned} \lim_{z\mapsto z_i^-}\Theta_i(t,z) &= \lim_{z\mapsto z_i^+}\Theta_{i+1}(t,z), \\ \lim_{z\mapsto z_i^-}\kappa_i\left(\Theta_i(t,z)\right)\frac{\partial \Theta_i(t,z)}{\partial z} &= \lim_{z\mapsto z_i^+}\kappa_{i+1}\left(\Theta_{i+1}(t,z)\right)\frac{\partial \Theta_{i+1}(t,z)}{\partial z}, \end{aligned}\right\} \tag{4}$$

for $t>0$ and $i=1,2,\ldots,m-1$. From the compatibility condition (4) a single function $\Theta(t,z)$ can be used instead of the m functions $\Theta_i(t,z)$:

$$\Theta(t,z)=\Theta_i(t,z), \qquad z_{i-1}\leq z\leq z_i.$$

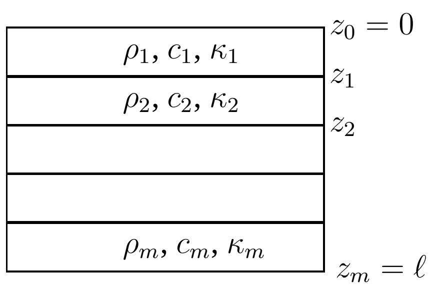

Fig. 3.

A new function denoted with $u(t)$ is defined

$$u(t)=\sum_{i=1}^{m}\int_{z_{i-1}}^{z_i}\rho_i(\Theta(t,z))c_i(\Theta(t,z))\Theta(t,z)\,dz, \tag{5}$$

which is dimensionally $[J/m^2]$, and by using (3) and (4) its total time derivative becomes:

$$\frac{du(t)}{dt}=\dot{q}_s(t)-\dot{q}_b(t), \tag{6}$$

where

$$\dot{q}_s(t) = -\kappa_1(\Theta(t,0)) \left.\frac{\partial\Theta(t,z)}{\partial z}\right|_{z=0}, \qquad \dot{q}_b(t) = -\kappa_m(\Theta(t,\ell)) \left.\frac{\partial\Theta(t,z)}{\partial z}\right|_{z=\ell} \tag{7}$$

and $\dot{q}_s(t)$ is the *impinging convective heat flux rate* while $\dot{q}_b(t)$ is the *backface convective heat flux rate*.

The differential equation (3) is closed by the initial temperature distribution $\Theta^{init}(z)$;

$$\Theta(0,z) = \Theta^{init}(z), \qquad 0 \le z \le \ell$$

and boundary conditions: at the surface, i.e. $z = 0$ either temperature or heat flux rate can be set for all $t > 0$;

$$\Theta(t,0) = \Theta^s(t), \qquad \text{if } \Theta^s(t) \text{ is given} \tag{8.a}$$

$$\kappa_1(\Theta(t,0)) \left.\frac{\partial\Theta(t,z)}{\partial z}\right|_{z=0} = -\dot{q}_s(t), \qquad \text{if } \dot{q}_s(t) \text{ is given} \tag{8.b}$$

Analogously on the back surface, i.e. $z = \ell$;

$$\Theta(t,\ell) = \Theta^\ell(t), \qquad \text{if } \Theta^\ell(t) \text{ is given} \tag{9.a}$$

$$\kappa_n(\Theta(t,\ell)) \left.\frac{\partial\Theta(t,z)}{\partial z}\right|_{z=\ell} = -\dot{q}_b(t), \qquad \text{if } \dot{q}_b(t) \text{ is given} \tag{9.b}$$

As a temperature signal $\Theta^s(t)$ is assigned, it is possible to solve the differential equation (3) with surface boundary condition (8.a) to obtain the body temperature distribution $\Theta(t,z)$ and by heat rate (7) $\dot{q}_s(t)$ is thus evaluated. By the solution $\Theta(t,z)$, h can be rewritten as follows

$$h = -\kappa_1(\Theta(t,0)) \left.\frac{\partial\Theta(t,z)}{\partial z}\right|_{z=0} \left(\Theta^\infty(t) - \Theta(t,0)\right)^{-1}. \tag{10}$$

Only in few simple cases $\Theta(t,z)$ can be computed exactly, and generally it must be approximated by means of numerical techniques.

It is worth to note that equation (10) do not define a single value for h but it is most generally a function of the time.

Approximation of h can be affected from several error sources, among them we recall:

- errors in the measurements of $\Theta^s(t)$ and $\Theta^\infty(t)$.

- errors in the estimation of $\dot{q}_s(t)$ due to numerical procedure and accuracy of the physical model.

Naming h_e an estimation of the *true* heat transfer coefficient one of the following approaches can be used for its evaluation:

A: Direct method. Given $\Theta^s(t)$ and $\Theta^\infty(t)$ compute $\Theta(t,z)$ and $H(t)$ defined as

$$H(t) = -\kappa_1(\Theta(t,0)) \left.\frac{\partial\Theta(t,z)}{\partial z}\right|_{z=0} (\Theta^\infty(t) - \Theta(t,0))^{-1},$$

and using some regression on $H(t)$ estimate h. Some noise reduction procedure has to be adopted.

B: Indirect method. From (10) the surface boundary condition becomes

$$-\kappa_1(\Theta(t,0)) \left.\frac{\partial\Theta(t,z)}{\partial z}\right|_{z=0} = h\,(\Theta^\infty(t) - \Theta(t,0)). \tag{11}$$

For each prescribed h, equation (3) together with equation (11) constitute a functional equation which solutions is a temperature history $\Theta_h(t,z)$. Among all the possible $\Theta_h(t,z)$ the one which "best fits" the measured temperature signal is finally chosen.

Notice that both approaches need the knowledge of an approximation procedure in order to estimate $\Theta(t,z)$. In the following section the principal ones are recalled.

5 One layer slab

In this case the slab has everywhere constant physical properties so that the indices in ρ_1, c_1 and κ_1 are omitted. If the test duration is short enough and/or the thickness of the slab is properly chosen, the finite slab can be modeled by a semi-infinite ones. Moreover, if the temperature inside the slab do not increase too much the following approximations hold:

$$\rho(\Theta) \equiv \rho, \qquad c(\Theta) \equiv c, \qquad \kappa(\Theta) \equiv \kappa, \tag{12}$$

i.e. their values are assumed constant and evaluated at the initial temperature. This is the case when the diffusivity of the layer is sufficiently low or the impinged heat flux is moderate.

The one dimensional semi-infinite slab with (12) can be modeled by the following linear partial differential equation

$$\rho c \frac{\partial \Theta(t,z)}{\partial t} = \kappa \frac{\partial^2 \Theta(t,z)}{\partial z^2}, \qquad t > 0, \quad z > 0 \tag{13}$$

with the following boundary conditions

$$\Theta(t,0) = \Theta^s(t), \qquad \lim_{z \mapsto \infty} \frac{\partial \Theta(t,z)}{\partial z} = 0, \tag{14}$$

for $t > 0$. The slab is assumed to be in thermal equilibrium at $t = 0$ so that (without loss of generality) the following initial condition is given as initial condition:

$$\Theta(0,z) = 0, \qquad z \geq 0. \tag{15}$$

With assumption (12)–(14)–(15) the equation (13) can be easily solved by means of the Laplace transform as follows: Let $\Delta\Theta$ the Laplace transform respect to time of Θ, so that equation (13) become

$$\rho c s \Delta\Theta(s,z) = \kappa \frac{\partial^2 \Delta\Theta(s,z)}{\partial z^2}, \qquad \lim_{z \mapsto \infty} \frac{\partial \Delta\Theta(s,z)}{\partial z} = 0,$$

which has the following solution:

$$\Delta\Theta(s,z) = \Delta\Theta(s,0) \exp\left(-z \left(\frac{\rho c s}{\kappa}\right)^{1/2}\right), \tag{16}$$

and from (16) with the boundary condition (7) it is possible to write

$$\Delta\dot{q}_s(s) = -\kappa \left. \frac{\partial \Delta\Theta(s,z)}{\partial z} \right|_{z=0} = s^{1/2} \, (\rho c \kappa)^{1/2} \, \Delta\Theta(s,0). \tag{17}$$

Taking the inverse Laplace transform of (17), one can express $\dot{q}_s(t)$ in function of $\Theta(t,0)$ or vice versa by the following equations:

$$\dot{q}_s(t) = \frac{(\rho c \kappa)^{1/2}}{\pi^{1/2}} \int_0^t \frac{\left.\frac{\partial \Theta(t,0)}{\partial t}\right|_{t=\tau}}{(t-\tau)^{1/2}} \, d\tau, \tag{18.a}$$

$$\Theta(t,0) = \frac{1}{\pi^{1/2} \, (\rho c \kappa)^{1/2}} \int_0^t \frac{\dot{q}_s(\tau)}{(t-\tau)^{1/2}} \, d\tau. \tag{18.b}$$

Two kind of difficulties arise either for numerical or algebraic approximation of equations (18.a)-(18.b):

(1) The surface temperature $\Theta(t,0)$ is normally known only at discrete time t_i according with the acquisition frequency of the DAS system.
(2) The computation of $\dot{q}_s(t)$ for a given $\Theta(t,0)$ is not straightforward.

5.1 Heaveside like heat flux approximation

In many practical situation the heat signal $\dot{q}_s(t)$ shows a sudden increase in a short initial time (rise time) and thereafter drops with a approximatively a constant slope. In this situation it is possible to produce, for a given temperature signal, an approximate formula for $\dot{q}_s(t)$. Formula (18.b) can be rewritten as

$$
\begin{aligned}
\pi^{1/2}\,(\rho c\kappa)^{1/2}\,\Theta(t,0) &= \int_0^t \frac{\dot{q}_s(\tau)-\dot{q}_s(t)+\dot{q}_s(t)}{(t-\tau)^{1/2}}\,d\tau, \\
&= \int_0^t \frac{\dot{q}_s(t)}{(t-\tau)^{1/2}}\,d\tau + \int_0^t \frac{\dot{q}_s(\tau)-\dot{q}_s(t)}{(t-\tau)^{1/2}}\,d\tau, \\
&= 2\dot{q}_s(t)t^{1/2} + 2t^{1/2}E(t),
\end{aligned}
$$

where

$$
E(t) = \frac{1}{2t^{1/2}}\int_0^t \frac{\dot{q}_s(\tau)-\dot{q}_s(t)}{(t-\tau)^{1/2}}\,d\tau.
$$

So it is possible to write

$$
\dot{q}_s(t) + E(t) = \frac{\pi^{1/2}\,(\rho c\kappa)^{1/2}}{2}\frac{\Theta(t,0)}{t^{1/2}},
$$

and this relation suggests the following approximation

$$
\dot{q}_s(t) \approx \frac{\pi^{1/2}\,(\rho c\kappa)^{1/2}}{2}\frac{\Theta(t,0)}{t^{1/2}}, \tag{19}
$$

where $E(t)$ becomes the absolute error in this approximation. The applications of the above solution requires an accurate determination of the time origin of the parabolic temperature time trace.

The absolute error $E(t)$ satisfies

$$
\begin{aligned}
|E(t)| &= \left| \frac{1}{2t^{1/2}} \int_0^t \frac{\dot{q}_s(\tau) - \dot{q}_s(t)}{(t-\tau)^{1/2}}\, d\tau \right|, \\
&\le \left| \frac{1}{2t^{1/2}} \int_0^{t_H} \frac{\dot{q}_s(\tau) - \dot{q}_s(t)}{(t-\tau)^{1/2}}\, d\tau \right| + \left| \frac{1}{2t^{1/2}} \int_{t_H}^{t} \frac{\dot{q}_s(\tau) - \dot{q}_s(t)}{(t-\tau)^{1/2}}\, d\tau \right|, \qquad (20) \\
&\le M_1 \left(\frac{t_H}{t} \right)^{1/2} + M_2,
\end{aligned}
$$

where

$$
\begin{aligned}
M_1 &= 2 \sup_{x \in [0, t_H]} |\dot{q}_s(x)|, \\
M_2 &= \sup_{x,y \in [t_H, t]} |\dot{q}_s(x) - \dot{q}_s(y)|.
\end{aligned}
$$

Constant M_1 is of the order of the maximum recorded heat flux, while constant M_2 is proportional to the heat fluctuation after the initial raise time. It can be noticed in formula (20) that for t small the error is dominated by $M_1 (t_H/t)^{1/2}$ so that approximation (19) is apparently good for $t \gg t_H$ and if the rise time t_H is short compared to the total test duration. Formula (20) gives a guide rule design for time assessment.

5.2 The Cook and Felderman method

The Cook and Felderman (1966) method is based on a piecewise linear approximation of the surface temperature $\Theta(t, 0)$ introduced to reconstruct temperature signal known at discrete times. Moreover such an approximation of temperature signal simplifies the approximate computation of integral (18.a). A linear spline $\Theta^L(t)$ which interpolates $\Theta_i = \Theta(t_i, 0)$ is build as below:

$$
\Theta^L(\tau) = \frac{(\tau - t_{i-1})\Theta_i + (t_i - \tau)\Theta_{i-1}}{t_i - t_{i-1}}, \qquad t_{i-1} \le \tau \le t_i. \qquad (21)
$$

for $i = 1, 2, \ldots, n_s - 1$ where n_s is the total number of sampled temperatures with $t_0 = 0$. Substitution of (21) in formula (18.a) with $t = t_m$ produces an approximate values for $\dot{q}_s(t_m)$. This approximation is known as the Cook and Felderman method.

Observe that

$$\frac{d\Theta^L(\tau)}{d\tau} = \frac{\Theta_i - \Theta_{i-1}}{t_i - t_{i-1}}, \qquad t_{i-1} < t < t_i, \tag{22}$$

and that (22) is not defined for $\tau = t_i$ (the nodal points). In order to evaluate the error of Cook and Felderman approximation the following expression for the error (simply obtained from Taylor series) of the approximation of the time derivative is used the following formula

$$\frac{\partial\Theta(t,0)}{\partial t} = \frac{\Theta_i - \Theta_{i-1}}{t_i - t_{i-1}} + E_i(t)(t_i - t_{i-1}), \qquad t_{i-1} < t < t_i, \tag{23}$$

where

$$|E_i(t)| \leq \frac{1}{2} \max_{t\in[t_{i-1},t_i]} \left|\frac{\partial^2\Theta(t,0)}{\partial t^2}\right|. \tag{24}$$

Substituting (23) in (18.a)

$$\begin{aligned} \dot{q}_s(t_j) = {} & \frac{(\rho c\kappa)^{1/2}}{\pi^{1/2}} \sum_{i=1}^{j} \int_{t_{i-1}}^{t_i} \frac{\Theta_i - \Theta_{i-1}}{t_i - t_{i-1}} \frac{1}{(t_j - \tau)^{1/2}}\, d\tau \\ & + \frac{(\rho c\kappa)^{1/2}}{\pi^{1/2}} \sum_{i=1}^{j} \int_{t_{i-1}}^{t_i} \frac{E_i(t)(t_i - t_{i-1})}{(t_j - \tau)^{1/2}}\, d\tau, \end{aligned}$$

we have

$$\dot{q}_s(t_j) = 2\frac{(\rho c\kappa)^{1/2}}{\pi^{1/2}} \sum_{i=1}^{j} \frac{\Theta_i - \Theta_{i-1}}{(t_j - t_i)^{1/2} + (t_j - t_{i-1})^{1/2}} + \frac{(\rho c\kappa)^{1/2}}{\pi^{1/2}} E(t_j), \tag{25}$$

where

$$\begin{aligned} |E(t_j)| &= \left|\sum_{i=1}^{j} \int_{t_{i-1}}^{t_i} \frac{E_i(t)(t_i - t_{i-1})}{(t_j - \tau)^{1/2}}\, d\tau\right| \\ &\leq \left|\sum_{i=1}^{j} \int_{t_{i-1}}^{t_i} \frac{t_i - t_{i-1}}{(t_j - \tau)^{1/2}}\, d\tau\right| \frac{1}{2} \max_{t\in[0,t_j]} \left|\frac{\partial^2\Theta(t,0)}{\partial t^2}\right|, \\ &\leq \max_{t\in[0,t_j]} \left|\frac{\partial^2\Theta(t,0)}{\partial t^2}\right| \sum_{i=1}^{j} \frac{(t_i - t_{i-1})^2}{(t_j - t_{i-1})^{1/2} + (t_j - t_i)^{1/2}}. \end{aligned} \tag{26}$$

The Cook and Felderman approximation is obtained from (25) by neglecting the error term $E(t_m)$ so that denoting by $\dot{q}_{sm}$ the approximation of $\dot{q}_s(t_m)$ it follows

$$\boxed{\dot{q}_s(t_j) \approx \dot{q}_{sj} = 2\frac{(\rho c\kappa)^{1/2}}{\pi^{1/2}} \sum_{i=1}^{j} \frac{\Theta_i - \Theta_{i-1}}{(t_j - t_i)^{1/2} + (t_j - t_{i-1})^{1/2}}.} \tag{27}$$

This last form is the equation usually implemented in heat transfer data reduction programs subjected only to the assumption of the one dimensional heat conduction in a semi-infinite slab with constant thermal properties.

In order to obtain a more simple estimate of $E(t_m)$ the following constant is defined:

$$\Delta t = \max_{i=1,2,..,n_s} t_i - t_{i-1},$$

set from (26) the following estimate holds

$$\begin{aligned} |E(t_j)| &\leq \max_{t\in[0,t_j]} \left| \frac{\partial^2\Theta(t,0)}{\partial t^2} \right| \sum_{i=1}^{j} \frac{(t_i - t_{i-1})^2}{t_i - t_{i-1}} \left((t_j - t_{i-1})^{1/2} - (t_j - t_i)^{1/2} \right), \\ &\leq \max_{t\in[0,t_j]} \left| \frac{\partial^2\Theta(t,0)}{\partial t^2} \right| \Delta t \sum_{i=1}^{j} \left((t_j - t_{i-1})^{1/2} - (t_j - t_i)^{1/2} \right), \\ &\leq \max_{t\in[0,t_j]} \left| \frac{\partial^2\Theta(t,0)}{\partial t^2} \right| \Delta t t_j^{1/2}, \end{aligned}$$

From this inequality it is evident that Cook and Felderman is at least a first order scheme.

Remark 1 *From* (27) *and the following manipulation*

$$\begin{aligned} &\sum_{i=1}^{j} \frac{\Theta_i - \Theta_{i-1}}{(t_j - t_{i-1})^{1/2} + (t_j - t_i)^{1/2}} \\ &\quad = \sum_{i=1}^{j} \frac{\Theta_i - \Theta_{i-1}}{t_i - t_{i-1}} \left((t_j - t_{i-1})^{1/2} - (t_j - t_i)^{1/2} \right) \\ &\quad = \sum_{i=1}^{j} \frac{\Theta_i - \Theta_{i-1}}{t_i - t_{i-1}} (t_j - t_{i-1})^{1/2} - \sum_{i=1}^{j} \frac{\Theta_i - \Theta_{i-1}}{t_i - t_{i-1}} (t_j - t_i)^{1/2} \\ &\quad = \sum_{i=0}^{j-1} \frac{\Theta_{i+1} - \Theta_i}{t_{i+1} - t_i} (t_j - t_i)^{1/2} - \sum_{i=1}^{j} \frac{\Theta_i - \Theta_{i-1}}{t_i - t_{i-1}} (t_j - t_i)^{1/2} \\ &\quad = \sum_{i=1}^{j-1} \left(\frac{\Theta_{i+1} - \Theta_i}{t_{i+1} - t_i} - \frac{\Theta_i - \Theta_{i-1}}{t_i - t_{i-1}} \right) (t_j - t_i)^{1/2} + \frac{\Theta_1 - \Theta_0}{t_1 - t_0} (t_j - t_0)^{1/2} \end{aligned}$$

by setting $\Theta_{-1} = \Theta_0$ *and* t_{-1} *any number less than* t_0 *previous formula becomes*

$$\sum_{i=1}^{j} \frac{\Theta_i - \Theta_{i-1}}{(t_j - t_{i-1})^{1/2} + (t_j - t_i)^{1/2}} = \sum_{i=0}^{j-1} \left(\frac{\Theta_{i+1} - \Theta_i}{t_{i+1} - t_i} - \frac{\Theta_i - \Theta_{i-1}}{t_i - t_{i-1}} \right) (t_j - t_i)^{1/2} \quad (28)$$

when sampling rate is constant i.e. $t_i - t_{i-1} = \Delta t$ *for all* i *equation* (28) *substituted* *in* (27) *reduce to*

$$\boxed{\dot{q}_s(t_j) \approx \dot{q}_{sj} = 2\frac{(\rho c \kappa)^{1/2}}{\pi^{1/2}\Delta t^{1/2}} \sum_{i=0}^{j-1} (\Theta_{i+1} - 2\Theta_i + \Theta_{i-1})\,(j-i)^{1/2}}$$

which is the scheme differently deduced from Oldfield et al. (1978).

5.3 Implicit Cook and Felderman

An implicit version of Cook and Felderman is based on a piecewise constant approximation of the surface heat $\dot{q}_s(t)$. A piecewise constant spline $\dot{q}^L(t)$ is build as below:

$$\dot{q}^L(\tau) = \dot{q}_{s\,i-\frac{1}{2}}, \qquad t_{i-1} \leq \tau \leq t_i. \tag{29}$$

Substitution of (29) in formula (18.b) instead of $\dot{q}_s(t)$ produce for $t = t_m$ an approximate values for $\Theta(t_j, 0)$.

$$\Theta(t_j, 0) \approx \frac{2}{\pi^{1/2}\,(\rho c \kappa)^{1/2}} \sum_{i=1}^{j} \left((t_j - t_{i-1})^{1/2} - (t_j - t_i)^{1/2} \right) \dot{q}_{s\,i-\frac{1}{2}}, \tag{30}$$

which for all $j > 0$ is an implicit linear relation in the unknown $\dot{q}_{s\,i-\frac{1}{2}}$. Assuming equality in (30) the following recurrence is produced:

$$\begin{aligned}
\dot{q}_{s\,\frac{1}{2}} &= \frac{\pi^{1/2}\,(\rho c \kappa)^{1/2}\;\Theta(t_1, 0)}{2\,(t_1 - t_0)^{1/2}} \qquad (31)\\
&\;\vdots\\
\dot{q}_{s\,k-\frac{1}{2}} &= \frac{\pi^{1/2}\,(\rho c \kappa)^{1/2}\;\Theta(t_k, 0) - 2\displaystyle\sum_{i=1}^{k-1} \left((t_k - t_{i-1})^{1/2} - (t_k - t_i)^{1/2} \right) \dot{q}_{s\,i-\frac{1}{2}}}{2\,(t_k - t_{k-1})^{1/2}}\\
&\;\vdots
\end{aligned}$$

5.4 *Algebraic method*

Algebraic methods assume h constant. The free stream temperature behaves as follows

$$\Theta^{\infty}(t) = \begin{cases} 0 & \text{if } t < 0 \\ \\ \Theta^{\infty} & \text{if } t \geq 0 \end{cases} \tag{32}$$

Such an assumption implies a sudden change in the fluid dynamic and thermal characteristics of the flow.
From equation (13) with conditions (12)–(14)–(15)–(32) it follows

$$\dot{q}_s(t) = h\left(\Theta^{\infty}(t) - \Theta(t,0)\right). \tag{33}$$

and by taking the Laplace transform of (33) together with (17) the following equality can be written

$$s^{1/2}\ (\rho c \kappa)^{1/2}\ \Delta\Theta(s,0) = h\left(\frac{\Theta^{\infty}}{s} - \Delta\Theta(s,0)\right),$$

so that

$$\Delta\Theta(s,0) = \frac{\Theta^{\infty}}{s}\left(1 + s^{1/2}\ \left(\frac{\rho c \kappa}{h}\right)^{1/2}\right)^{-1}. \tag{34}$$

Taking the inverse Laplace transform of (34) it follows

$$\Theta(t,0) = \Theta^{\infty}\phi(t\beta), \qquad \beta = \frac{h^2}{\rho c \kappa}, \tag{35}$$

where

$$\begin{aligned} \phi(x) &= 1 - \exp(x)\,\mathrm{erfc}\left(x^{1/2}\right), \\ \mathrm{erfc}\,(x) &= 1 - \mathrm{erf}\,(x)\,, \\ \mathrm{erf}\,(x) &= \frac{2}{\pi^{1/2}}\int_{-\infty}^{x} \exp\left(-\omega^2\right)\,d\omega. \end{aligned}$$

Equation (35) models the temperature rise on the surface of the slab under the assumption that the heat transfer coefficient is a *constant*. Equation (35) defines a functions family parameterized by h. Within such a family one get the best fit of the measured signal $\Theta^s(t_i)$ with $i = 0, 1, \ldots, m$. A possible way to select h is the following: set

$$
\begin{aligned}
g(\beta) &= \sum_{i=0}^{m} \Theta^s(t_i)\delta t_i - \sum_{i=1}^{m} \Theta(t_i,0)\delta t_i \\
&= \sum_{i=0}^{m} \Theta^s(t_i)\delta t_i - \Theta^\infty \sum_{i=0}^{m} \phi(t_i\beta)\delta t_i
\end{aligned}
$$

where

$$
\delta t_i = \frac{1}{2}\begin{cases} t_1 - t_0 & \text{if } i = 0 \\ t_{i+1} - t_{i-1} & \text{if } 0 < i < m \\ t_m - t_{m-1} & \text{if } i = m \end{cases}
$$

The value of β such that $g(\beta) = 0$ corresponds to the temperature distribution which generates the same amount of heat as produced by the real temperature signal estimated by trapezoidal quadrature rule. Observing now that

$$
g'(\beta) = -\Theta^\infty \sum_{i=0}^{m} \phi'(t_i\beta)t_i\delta t_i, \qquad \phi'(x) = \frac{1}{\pi x^{1/2}} - \exp(x)\,\mathrm{erfc}\left(x^{1/2}\right),
$$

and $\phi'(x) > 0$ for $x > 0$ it results that $g(\beta)$ is a monotone decreasing function of β, moreover

$$
g(0) = \sum_{i=0}^{m} \Theta^s(t_i)\delta t_i > 0, \qquad g(+\infty) = -\infty
$$

so that there is a unique β such that $g(\beta) = 0$. Because $g(x) < 0$ for all $x > 0$ Newton-Raphson scheme, for example, can be used to approximate β and consequently h.

6 Two layer slab

If the test duration is short enough and/or the thickness of the slab is properly chosen the finite size second layer, can be approximated by a semi-infinite ones. According with the consideration in section 5 if the temperature inside the slab do not increase too much the following assumption can be done

$$
\rho_i(\Theta) \equiv \rho_i, \qquad c_i(\Theta) \equiv c_i, \qquad \kappa_i(\Theta) \equiv \kappa_i, \qquad i = 1,2 \tag{36}
$$

i.e. their values are assumed constant and evaluated at the initial temperature.

The one dimensional semi-infinite slab with (36) can be modeled by the following partial differential equations

$$\begin{aligned} \rho_1 c_1 \frac{\partial \Theta(t,z)}{\partial t} &= \kappa_1 \frac{\partial^2 \Theta(t,z)}{\partial z^2}, \qquad t>0, \quad 0<z<z_1 \\ \rho_2 c_2 \frac{\partial \Theta(t,z)}{\partial t} &= \kappa_2 \frac{\partial^2 \Theta(t,z)}{\partial z^2}, \qquad t>0, \quad z>z_1 \end{aligned} \tag{37}$$

being $\Theta(t,z)$ a continuous function with the following internal condition

$$\kappa_1 \lim_{z \mapsto z_1^-} \frac{\partial \Theta(t,z)}{\partial z} = \kappa_2 \lim_{z \mapsto z_1^+} \frac{\partial \Theta(t,z)}{\partial z}, \qquad t>0 \tag{38}$$

and the following boundary conditions

$$\Theta(t,0) = \Theta^s(t), \qquad \lim_{z \mapsto \infty} \frac{\partial \Theta(t,z)}{\partial z} = 0, \qquad t>0 \tag{39}$$

The slab is assumed to be in thermal equilibrium at time $t=0$, so that (without loss of generality) the following initial condition arises:

$$\Theta(0,z) = 0, \qquad z \geq 0 \tag{40}$$

With assumption (36)-(38)-(39)-(40) the equations (37) are linear and can be solved by means of the Laplace transform and $\Delta\dot{q}_s(s)$ can be correlated with $\Delta\Theta(s,0)$ as follows

$$\Delta\dot{q}_s(s) = \Delta\Theta(s,0) \left(\rho_1 c_1 \kappa_1\right)^{1/2} \; s^{1/2} \frac{1 - A \exp\left(-2 s^{1/2} \tau_1^{1/2}\right)}{1 + A \exp\left(-2 s^{1/2} \tau_1^{1/2}\right)}, \tag{41}$$

being

$$A = \frac{\left(\rho_1 c_1 \kappa_1\right)^{1/2} - \left(\rho_2 c_2 \kappa_2\right)^{1/2}}{\left(\rho_1 c_1 \kappa_1\right)^{1/2} + \left(\rho_2 c_2 \kappa_2\right)^{1/2}}, \qquad \tau_1 = z_1^2 \frac{\rho_1 c_1}{\kappa_1} = \frac{z_1^2}{\alpha_1}.$$

Observing that

$$\frac{1 + \sigma \exp\left(-2 s^{1/2} \tau_1^{1/2}\right)}{1 - \sigma \exp\left(-2 s^{1/2} \tau_1^{1/2}\right)} = 1 + 2 \sum_{n=1}^{\infty} \sigma^n \exp\left(-2 n s^{1/2} \tau_1^{1/2}\right),$$

it is possible to invert the Laplace transform for (41) obtaining $\dot{q}_s(t)$ as a function of $\Theta(t,0)$ or $\Theta(t,0)$ in function of $\dot{q}_s(t)$ respectively as follows

$$\dot{q}_s(t) = \frac{(\rho_1 c_1 \kappa_1)^{1/2}}{\pi^{1/2}} \int_0^t \left.\frac{\partial\Theta(t,0)}{\partial t}\right|_{t=\tau} \frac{\Omega\left(-A, t-\tau\right)}{(t-\tau)^{1/2}}\, d\tau, \tag{42.a}$$

$$\Theta(t,0) = \frac{1}{\pi^{1/2}\left(\rho_1 c_1 \kappa_1\right)^{1/2}} \int_0^t \dot{q}_s(\tau) \frac{\Omega\left(A, t-\tau\right)}{(t-\tau)^{1/2}}\, d\tau, \tag{42.b}$$

where

$$\Omega\left(\sigma, x\right) = 1 + 2\sum_{n=1}^{\infty} \sigma^n \mathrm{exp}\left(-\frac{n^2\tau_1}{x}\right).$$

Notice that in the case $\sigma = 0$ the function $\Omega\left(\sigma, x\right)$ is identically equal to 1. Observe that when $A = 0$ the two layer slab behaves as a single layer. This is the case when the two layers are made of the same materials or when they have the same thermal product.

6.1 *Heaveside like heat flux approximation for two layer slab*

When a sudden change of the thermo-fluid dynamic characteristics of the free stream occurs it is possible to produce, for a given temperature signal, an approximate formula for $\dot{q}_s(t)$. Formula (42.b) can be rewritten as

$$\begin{aligned}
\pi^{1/2}\left(\rho_1 c_1 \kappa_1\right)^{1/2}\Theta(t,0) &= \int_0^t \frac{\dot{q}_s(\tau) - \dot{q}_s(t) + \dot{q}_s(t)}{(t-\tau)^{1/2}} \Omega\left(A, t-\tau\right) d\tau, \qquad (43)\\
&= \int_0^t \frac{\dot{q}_s(t)}{(t-\tau)^{1/2}} \Omega\left(A, t-\tau\right) d\tau + \int_0^t \frac{\dot{q}_s(\tau) - \dot{q}_s(t)}{(t-\tau)^{1/2}} \Omega\left(A, t-\tau\right) d\tau,\\
&= \dot{q}_s(t)\left\{2t^{1/2} + 4\sum_{n=1}^{\infty} A^n \left[t^{1/2}\,\mathrm{exp}\left(-(nz)^2\right) + n\tau_1^{1/2}\pi^{1/2}\,\mathrm{erf}\left(nz\right)\right]\right\}\\
&\quad + 2t^{1/2}E(t),
\end{aligned}$$

where $z = \tau_1/t$ and

$$E(t) = \frac{1}{2t^{1/2}} \int_0^t \frac{\dot{q}_s(\tau) - \dot{q}_s(t)}{(t-\tau)^{1/2}} \Omega\left(A, t-\tau\right) d\tau.$$

Following Pelle and Arts 1997, relation (43) can be roughly approximated by:

$$\dot{q}_s(t) \approx \Theta(t,0) \begin{cases} \left[\dfrac{2t^{1/2}}{\pi^{1/2} \left(\rho_1 c_1 \kappa_1\right)^{1/2}} \right]^{-1} & \text{for } t < t^* \\ \left[\dfrac{2t^{1/2}}{\pi^{1/2} \left(\rho_2 c_2 \kappa_2\right)^{1/2}} + \dfrac{z_1}{\kappa_1} \left(1 - \dfrac{\rho_1 c_1 \kappa_1}{\rho_2 c_2 \kappa_2} \right) \right]^{-1} & \text{for } t > t^* \end{cases},$$

where

$$t^* = \frac{\pi^{1/2}}{2} \frac{z_1}{\kappa_1} \frac{\left(\rho_1 c_1 \kappa_1\right)^{1/2}}{\left(\rho_2 c_2 \kappa_2\right)^{1/2}}.$$

6.2 A Cook and Felderman like method

As for the Cook and Felderman method the surface temperature $\Theta(t,0)$ is approximated by a linear spline as in (21). Substitution of (21) in formula (42.a) produces

$$\dot{q}_s(t_j) = \frac{\left(\rho_1 c_1 \kappa_1\right)^{1/2}}{\pi^{1/2}} \sum_{i=1}^{j} \frac{\Theta_i - \Theta_{i-1}}{t_i - t_{i-1}} \int_{t_{i-1}}^{t_i} \frac{\Omega\left(-A, t_j - \tau\right)}{\left(t_j - \tau\right)^{1/2}} \, d\tau + E(t_j) \tag{44}$$

where

$$E(t_j) = \frac{\left(\rho_1 c_1 \kappa_1\right)^{1/2}}{\pi^{1/2}} \sum_{i=1}^{j} \int_{t_{i-1}}^{t_i} \frac{E_i(t)(t_i - t_{i-1}) \Omega\left(-A, t_j - \tau\right)}{\left(t_j - \tau\right)^{1/2}} \, d\tau,$$

and $E_i(t)$ are defined in (24). The integral in (44) can be computed exactly:

$$C^j_{i-\frac{1}{2}} = \frac{1}{t_i - t_{i-1}} \int_{t_{i-1}}^{t_i} \frac{\Omega\left(-A, t_j - \tau\right)}{\left(t_j - \tau\right)^{1/2}} \, d\tau = -\frac{D^j_i - D^j_{i-1}}{t_i - t_{i-1}} \tag{45}$$

where

$$D^j_i = 2\left(t_j - t_i\right)^{1/2} + 4 \sum_{n=1}^{\infty} (-A)^n \left(\left(t_j - t_i\right)^{1/2} \exp\left(-\frac{n^2 \tau_1}{t_j - t_i} \right) + n \tau_1^{1/2} \pi^{1/2} \operatorname{erf}\left(n \frac{\tau_1^{1/2}}{\left(t_j - t_i\right)^{1/2}} \right) \right)$$

Substituting (45) into (44) the following equation is obtained

$$\dot{q}_s(t_j) = \sum_{i=1}^{j} C^j_{i-\frac{1}{2}} \left(\Theta_i - \Theta_{i-1}\right) + E(t_j) \tag{46}$$

The Cook and Felderman like approximation is obtained from (46) by neglecting the error term $E(t_j)$ so that denoting by $\dot{q}_{sj}$ the approximation of $\dot{q}_s(t_j)$ it follows

$$\boxed{\dot{q}_{sj} = \sum_{i=1}^{j} C^j_{i-\frac{1}{2}} \left(\Theta_i - \Theta_{i-1}\right)} \tag{47}$$

The error $E(t_j)$ becomes the absolute error in the previous approximation. As for the Cook and Felderman method an upper bound of this error can be estimated as follows

$$|E(t_j)| \leq \frac{\Delta t}{2} \max_{t\in[0,t_j]} \left| \frac{\partial^2 \Theta(t,0)}{\partial t^2} \right| \frac{(\rho_1 c_1 \kappa_1)^{1/2}}{\pi^{1/2}} \int_{t_0}^{t_j} \frac{\Omega(-A, t_j-\tau)}{(t_j-\tau)^{1/2}}\, d\tau,$$

observe that

$$\begin{aligned} D_0^j = \int_{t_0}^{t_j} \frac{\Omega(-A, t_j-\tau)}{(t_j-\tau)^{1/2}}\, d\tau &\leq 2t_j^{1/2} + 4\sum_{n=1}^{\infty} |-A|^n \left(t_j^{1/2} + n\pi^{1/2} tau_1^{1/2}\right) \\ &= 2\left(\frac{1+|A|}{1-|A|}\right) t_j^{1/2} + 4\frac{|A|}{(1-|A|)^2}\pi^{1/2}\tau_1^{1/2} \end{aligned}$$

and by

$$1+|A| = \frac{\max\left\{(\rho_1 c_1\kappa_1)^{1/2}, (\rho_2 c_2\kappa_2)^{1/2}\right\}}{(\rho_1 c_1\kappa_1)^{1/2} + (\rho_2 c_2\kappa_2)^{1/2}},$$

$$1-|A| = \frac{\min\left\{(\rho_1 c_1\kappa_1)^{1/2}, (\rho_2 c_2\kappa_2)^{1/2}\right\}}{(\rho_1 c_1\kappa_1)^{1/2} + (\rho_2 c_2\kappa_2)^{1/2}},$$

it follows

$$|E(t_j)| \leq \Delta t \frac{(\rho_1 c_1 \kappa_1)^{1/2}}{\pi^{1/2}} \left[C t_j^{1/2} + \frac{\pi^{1/2}\tau_1^{1/2}}{2}(C^2-1) \right],$$

where

$$C = \frac{\max\left\{(\rho_1 c_1\kappa_1)^{1/2}, (\rho_2 c_2\kappa_2)^{1/2}\right\}}{\min\left\{(\rho_1 c_1\kappa_1)^{1/2}, (\rho_2 c_2\kappa_2)^{1/2}\right\}},$$

so it is clear that (47) is at least a first order scheme.

Remark 2 *The computation on $C^j_{i-\frac{1}{2}}$ is very expensive due the presence of a series and the error function erf$(\cdot)$. An alternative approach is based on the following relation based on Lagrange and mean theorem:*

$$C^j_{i-\frac{1}{2}} = \frac{2 + 4\sum_{n=1}^{\infty}(-A)^n \left\{ \left(\frac{2n^2\tau_1}{x^2}+1\right) exp\left(-\frac{n^2\tau_1}{x^2}\right) - \frac{2n^2\tau_1}{z_0 z_1} exp\left(-\frac{n^2\tau_1}{y}\right) \right\}}{(t_j-t_i)^{1/2} + (t_j-t_{i-1})^{1/2}} \tag{48}$$

where $z_i = (t_j - t_i)^{1/2}$ and x and y are intermediate points in the interval $[z_i, z_{i-1}]$. If x and y are set to

$$x = y = z_i z_{i-1}$$

then (48) *is not an exact relation but it reduce to*

$$C^j_{i-\frac{1}{2}} \approx \frac{2+4\sum_{n=1}^{\infty}(-A)^n \mathit{exp}\left(-\frac{n^2\tau_1}{z_i z_{i-1}}\right)}{z_i^{1/2}+z_{i-1}^{1/2}},$$

where for $i=1$ *becomes*

$$C^j_{\frac{1}{2}} \approx \frac{2}{z_1^{1/2}}.$$

6.3 *Implicit Cook and Felderman like method*

A piecewise constant spline $\dot{q}^L(t)$ is build as in (29) and by substitution of (29) in formula (42.b) instead of $\dot{q}_s(t)$ produce for $t = t_j$ an approximate values for $\Theta(t_j, 0)$. The result is the following:

$$\begin{aligned} \Theta(t_j,0) &\approx \sum_{i=1}^{j}(t_i - t_{i-1}) I^j_{i-\frac{1}{2}} \dot{q}_{s\,i-\frac{1}{2}}, \\ I^j_{i-\frac{1}{2}} &= \frac{2+4\sum_{n=1}^{\infty}A^n \exp\left(-\frac{n^2\tau_1}{z_i z_{i-1}}\right)}{z_i^{1/2}+z_{i-1}^{1/2}}, \end{aligned} \tag{49}$$

which for all $j > 0$ is an implicit linear relation in the unknown $\dot{q}_{s\,i-\frac{1}{2}}$. Assuming equality in (49) the following recurrence is produced:

$$\begin{aligned} \dot{q}_{s\,\frac{1}{2}} &= \frac{\Theta(t_1,0)}{(t_1-t_0) I^1_{\frac{1}{2}}}, \\ &\vdots \\ \dot{q}_{s\,k-\frac{1}{2}} &= \frac{\Theta(t_k,0) - \sum_{i=1}^{k-1}(t_i - t_{i-1}) I^k_{i-\frac{1}{2}} \dot{q}_{s\,i-\frac{1}{2}}}{(t_k - t_{k-1}) I^k_{k-\frac{1}{2}}}, \\ &\vdots \end{aligned}$$

6.4 *Algebraic method for two layer slab*

Observing that

$$\dot{q}_{s\,j} \approx \dot{q}_s(t_j) = h\left(\Theta^{\infty}(t_j) - \Theta_j\right), \tag{50}$$

and combining (50) with (47) an approximation of Θ_j is obtained. Taking this approximation as an exact value it follows:

$$\Theta_j = \frac{h\Theta^\infty(t_j) + \sum_{i=1}^{j-1}(C^j_{i+\frac{1}{2}} - C^j_{i-\frac{1}{2}})\Theta_i}{h + C^j_{j-\frac{1}{2}}},$$

this last equation constitutes a recurrence relation that permits to compute the discrete surface temperature history Θ_j.

7 Multi layers slab

The methods based on Laplace transform become difficult to handle for $n > 2$ layers and are extremely costly for $n > 1$. Denoting with n_s the number of temperature samples, the cost of the Laplace Transform is of $\mathcal{O}\{n_s^2\}$. This computational cost can be reduced to $\mathcal{O}\{n_s \log n_s\}$ by using Fast Fourier transform based techniques. The precision of the approximate solution increases as the number of samples increases and for a large number of samples the excess of precision cannot be necessary. Thus, an alternative approach based on the finite elements approximation is here proposed which is simple to implement and more flexible. The basic solution algorithm can be used either to implement the direct or the indirect methods for an m-Layers finite size slab. Instead of write m differential equations as in (3) for $\Theta(t, z)$ the following functions can be defined

$$\begin{aligned}
\rho(z,\Theta) &= \rho_i(\Theta), \qquad z_{i-1} < z < z_i, \quad i = 1,2,\dots,m \\
c(z,\Theta) &= c_i(\Theta), \qquad z_{i-1} < z < z_i, \quad i = 1,2,\dots,m \qquad (51) \\
\kappa(z,\Theta) &= \kappa_i(\Theta), \qquad z_{i-1} < z < z_i, \quad i = 1,2,\dots,m
\end{aligned}$$

and using equations in (51) it is possible to rewrite both (3) and (4) in weak form as follows:

$$\int_0^{\ell}\left(\rho\left(z,\Theta(t,z)\right)c\left(z,\Theta(t,z)\right)\Phi(z)\frac{\partial\Theta(t,z)}{\partial t}+\kappa\left(z,\Theta(t,z)\right)\Phi'(z)\frac{\partial\Theta(t,z)}{\partial z}\right)dz$$
$$=\Phi(\ell)\kappa\left(\ell,\Theta(t,\ell)\right)\left.\frac{\partial\Theta(t,z)}{\partial z}\right|_{z=\ell}-\Phi(0)\kappa\left(0,\Theta(t,0)\right)\left.\frac{\partial\Theta(t,z)}{\partial z}\right|_{z=0} \tag{52}$$

The weak solution is the unique $\Theta(t,z)$ such that for all function Φ in an opportune functional space equation (52) is satisfied.

Due to the weak form of (52) the most natural way to approximate is the finite elements discretization.

7.1 The Finite Elements numerical scheme

The Finite Elements methods are widely used for the solutions of many kind of PDE (Zienkiewicz and Taylor; 1989) such as the parabolic ones in (52). This method is based on the approximation of the solution in a finite dimensional subspace, typically piecewise polynomials. In the present case the finite dimensional subspace is constructed as the space of piecewise linear spline in a partition of the interval $[0,\ell]$. The interval $[0,\ell]$ is partitioned in n subinterval not necessarily of the same size,

$$0=z_0<z_1<z_2<\cdots<z_{n-1}<z_n=\ell. \tag{53}$$

The partitions (53) is chosen in such a way that inside the intervals $[z_{i-1},z_i]$ the functions $\kappa(z,\Theta)$, $\rho(z,\Theta)$ and $c(z,\Theta)$ are constant respect to z so that the slab can be considered as composite of n layers. In general $n>m$ so that many of the original layers are split in others layers. Denoting with ρ_i, c_i and κ_i the corresponding function on the layer than

$$
\begin{aligned}
\rho(z,\Theta) &= \rho_i(\Theta), \qquad & z_{i-1} < z < z_i, \quad & i = 1,2,\ldots,n \\
c(z,\Theta) &= c_i(\Theta), \qquad & z_{i-1} < z < z_i, \quad & i = 1,2,\ldots,n \\
\kappa(z,\Theta) &= \kappa_i(\Theta), \qquad & z_{i-1} < z < z_i, \quad & i = 1,2,\ldots,n
\end{aligned}
$$

The temperature $\Theta(t,z)$ is approximated by using

$$
\Theta(t,z) \approx \sum_{i=0}^{n} \Theta_i(t)\phi_i(z), \tag{54}
$$

where

$$
\begin{gathered}
\phi_i(z) = \begin{cases} 0 & \text{if } z < z_{i-1} \\ \dfrac{z - z_{i-1}}{z_i - z_{i-1}} & \text{if } z_{i-1} \leq z \leq z_i \\ \dfrac{z_{i+1} - z}{z_{i+1} - z_i} & \text{if } z_i \leq z \leq z_{i+1} \\ 0 & \text{if } z > z_{i+1} \end{cases}, \\
\phi_0(z) = \begin{cases} \dfrac{z_1 - z}{z_1 - z_0} & \text{if } z \leq z_1 \\ 0 & \text{if } z < z_1 \end{cases}, \quad \phi_n(z) = \begin{cases} 0 & \text{if } z < z_{n-1} \\ \dfrac{z - z_{n-1}}{z_n - z_{n-1}} & \text{if } z \geq z_{n-1} \end{cases},
\end{gathered} \tag{55}
$$

using expansion (54) and standard finite elements approximation for (52) with base (55) and boundary condition (8.a) and (9.b) the following ODE is obtained:

$$
\begin{aligned}
&\Theta_0(t) = \Theta^s(t), \\
&\sum_{i=0}^{n} \Theta_i'(t) A_{ij}(\Theta) + \sum_{i=0}^{n} \Theta_i(t) B_{ij}(\Theta) = 0, \qquad j = 1,2,\ldots,n.
\end{aligned}
$$

The coefficients A_{ij} and B_{ij} results as following:

$$
\begin{aligned}
A_{ij}(\Theta) &= \int_0^{\ell} \rho\left(z, \Theta(t,z)\right) c\left(z, \Theta(t,z)\right) \phi_i(z)\phi_j(z)\, dz, \\
B_{ij}(\Theta) &= \int_0^{\ell} \kappa\left(z, \Theta(t,z)\right) \phi_i'(z)\phi_j'(z)\, dz.
\end{aligned} \tag{56}
$$

Trapezoidal quadrature rule is used instead of exact integrals for (56). The same A_{ij} and B_{ij} are used to denote such an approximation and takes the values:

$$A_{ij}(\Theta) = \begin{cases} M_i(\Theta_i) & \text{if } i = j \\ 0 & \text{otherwise} \end{cases},$$

$$B_{ij}(\Theta) = \begin{cases} -M_{i\pm\frac{1}{2}}(\Theta_i, \Theta_{i\pm 1}) & \text{if } j = i \pm 1 \\ M_{i+\frac{1}{2}}(\Theta_i, \Theta_{i+1})) + M_{i-\frac{1}{2}}(\Theta_{i-1}, \Theta_i) & \text{if } j = i \\ 0 & \text{otherwise} \end{cases},$$

where

$$\begin{aligned} M_0(\Theta_0) &= \rho_0(\Theta_0)c_0(\Theta_0)(z_1 - z_0)/2, \\ M_i(\Theta_i) &= \left(\rho_{i-1}(\Theta_i)c_{i-1}(\Theta_i)(z_i - z_{i-1}) + \rho_i(\Theta_i)c_i(\Theta_i)(z_{i+1} - z_i)\right)/2, \\ M_n(\Theta_n) &= \rho_{n-1}(\Theta_n)c_{n-1}(\Theta_n)(z_n - z_{n-1})/2, \\ M_{i+\frac{1}{2}}(\Theta_i, \Theta_{i+1}) &= \left(\kappa_i(\Theta_i) + \kappa_i(\Theta_{i+1})\right)/(2(z_{i+1} - z_i)), \end{aligned}$$

The semi-discrete discretization assume now the compact form:

$$\begin{aligned} \Theta_0(t) &= \Theta^s(t) \\ M_i(\Theta_i)\Theta_i'(t) &= M_{i+\frac{1}{2}}(\Theta_i, \Theta_{i+1})(\Theta_{i+1}(t) - \Theta_i(t)) \\ &\quad - M_{i-\frac{1}{2}}(\Theta_{i-1}, \Theta_i)(\Theta_i(t) - \Theta_{i-1}(t)), \\ M_n(\Theta_n)\Theta_n'(t) &= -M_{n-\frac{1}{2}}(\Theta_{n-1}, \Theta_n)(\Theta_n(t) - \Theta_{n-1}(t)), \end{aligned} \tag{57}$$

Equations (57) is a semi-discrete approximation of equation (52) and constitute a large system of initial value ordinary differential equations (ODE).

7.2 Time semi-implicit integrator

To solve system (57) any standard scheme for initial value ODE can be used. Consider the following ODE:

$$\begin{cases} \dfrac{dy}{dt} = f(t, y), \\ y(0) = y_0 \end{cases} \tag{58}$$

A simple scheme to approximate (58) is forward Euler scheme:

$$y^{n+1} = y^n + \Delta t f(t_n, y^n),$$

Explicit schemes suffers of instability and in particular explicit Euler scheme applied to ODE (57) can produce temperature oscillations. Implicit Euler scheme have good stability properties

$$y^{n+1} - \Delta t f(t_{n+1}, y^{n+1}) = y^n, \tag{59}$$

however y^{n+1} is not explicit and solution of (59) can be very time consuming. A simple modification of implicit Euler scheme results in a relatively cheap stable scheme. The resulting scheme by using the following shortcut

- Θ_i^j the approximation of $\Theta_i(t_j)$;
- $M_i^j = M_i(\Theta_i^j)$;
- $M_{i+\frac{1}{2}}^j = M_{i+\frac{1}{2}}(\Theta_i^j, \Theta_{i+1}^j)$;
- $\Delta t_j = t_{j+1} - t_j$

and applied to (57) is the following

$$\begin{aligned} \Theta_0^{j+1} &= \Theta^s(t_{j+1}) \\ \left(\frac{M_i^j}{\Delta t_j} + M_{i-\frac{1}{2}}^j + M_{i+\frac{1}{2}}^j\right)\Theta_i^{j+1} - M_{i-\frac{1}{2}}^j\Theta_{i-1}^{j+1} - M_{i+\frac{1}{2}}^j\Theta_{i+1}^{j+1} &= \frac{M_i^j}{\Delta t_j}\Theta_i^j, \\ \frac{M_n^j}{\Delta t_j}\Theta_n^{j+1} - M_{n-\frac{1}{2}}^j\Theta_{n-1}^{j+1} &= \frac{M_n^j}{\Delta t_j}\Theta_n^j, \end{aligned}$$

Notice that a fully implicit Euler scheme has M's coefficients computed at time t_{j+1} while this semi-implicit one has M's coefficient computed at time t_j. It is easy to see that the solution step involves the solution of a strictly diagonally dominant tridiagonal system with positive elements on the diagonal and non negative elsewhere. Then the coefficient matrix of the system is an M-matrix (see e.g. Axelsson (1994) for the definition). It is easy to prove that the discrete solution satisfies the discrete maximum principle (see Bertolazzi; 1998) so that the scheme is unconditionally stable. Moreover, if coefficients M's are independent of the temperature, the discrete solution have a discrete analog of conservation law (6). The role on the integral (5) is done by the discrete quantity:

$$\sum_{i=1}^{n} \frac{\rho_{i-1}(\Theta_{i-1}^j)c_{i-1}(\Theta_{i-1}^j) + \rho_{i-1}(\Theta_i^j)c_{i-1}(\Theta_i^j)}{2}(z_i - z_{i-1})$$

which is the trapezoidal approximation of (5). This means that there is no internal numerical loss or production of heat.

7.3 Algebraic Finite Elements method

According to the discretization procedure addressed in section 7.1 with this new boundary conditions:

$$\kappa(0)\left.\frac{\partial\Theta(t,z)}{\partial z}\right|_{z=0} = -\dot{q}_s(t) = -h(\Theta^\infty(t) - \Theta(t))$$
$$\kappa(\ell)\left.\frac{\partial\Theta(t,z)}{\partial z}\right|_{z=\ell} = 0,$$

for $t > 0$, the following ODE is obtained

$$\begin{aligned} M_0\Theta_0'(t) &= M_{\frac{1}{2}}(\Theta_1(t) - \Theta_0(t)) + h(\Theta^\infty(t) - \Theta_0(t)), \\ M_i\Theta_i'(t) &= M_{i+\frac{1}{2}}(\Theta_{i+1}(t) - \Theta_i(t)) - M_{i-\frac{1}{2}}(\Theta_i(t) - \Theta_{i-1}(t)), \\ M_n\Theta_n'(t) &= -M_{n-\frac{1}{2}}(\Theta_n(t) - \Theta_{n-1}(t)), \end{aligned}$$

As in section 7.1 the differential system can be approximated by a semi-implicit Euler scheme as follows:

$$\begin{gathered} \left(h + \frac{M_0^j}{\Delta t_j}\right)\Theta_0^{j+1} - M_{\frac{1}{2}}^j\Theta_1^{j+1} = \frac{M_0^j}{\Delta t_j}\Theta_0^j + h\Theta^\infty(t_{j+1}), \\ \left(\frac{M_i^j}{\Delta t_j} + M_{i-\frac{1}{2}}^j + M_{i+\frac{1}{2}}^j\right)\Theta_i^{j+1} - M_{i-\frac{1}{2}}^j\Theta_{i-1}^{j+1} - M_{i+\frac{1}{2}}^j\Theta_{i+1}^{j+1} = \frac{M_i^j}{\Delta t_j}\Theta_i^j, \\ \frac{M_n^j}{\Delta t_j}\Theta_n^{j+1} - M_{n-\frac{1}{2}}^j\Theta_{n-1}^{j+1} = \frac{M_n^j}{\Delta t_j}\Theta_n^j, \end{gathered} \tag{60}$$

By (60) for a given free stream temperature $\Theta^\infty(t)$ and a heat transfer coefficient h a temperature profile is generated. Since the discrete solution is parameterized by h the discrete temperatures Θ_i^j can be considered as function of h. Moreover the derivative $\dfrac{d\Theta_0^i}{dh}$ satisfies

$$\left(h+\frac{M_0^j}{\Delta t_j}\right)\frac{d\Theta_0^{j+1}}{dh}-M_{\frac{1}{2}}^j\frac{d\Theta_1^{j+1}}{dh}=\frac{M_0^j}{\Delta t_j}\frac{d\Theta_0^j}{dh}+\Theta^\infty(t_{j+1})-\Theta_0^{j+1},$$

$$\left(\frac{M_i^j}{\Delta t_j}+M_{i-\frac{1}{2}}^j+M_{i+\frac{1}{2}}^j\right)\frac{d\Theta_i^{j+1}}{dh}-M_{i-\frac{1}{2}}^j\frac{d\Theta_{i-1}^{j+1}}{dh}-M_{i+\frac{1}{2}}^j\frac{d\Theta_{i+1}^{j+1}}{dh}=\frac{M_i^j}{\Delta t_j}\frac{d\Theta_i^j}{dh},$$

$$\frac{M_n^j}{\Delta t_j}\frac{d\Theta_n^{j+1}}{dh}-M_{n-\frac{1}{2}}^j\frac{d\Theta_{n-1}^{j+1}}{dh}=\frac{M_n^j}{\Delta t_j}\frac{d\Theta_n^j}{dh},$$

this constitute a tridiagonal linear system in the unknown $\dfrac{d\Theta_i^{j+1}}{dh}$, the coefficient matrix is a diagonally dominant tridiagonal matrix with positive elements on the main diagonal and non positive elsewhere, thus it is an M-matrix. It is well known that an M-matrix is a monotone matrix i.e. all the components of its inverse are non-negative. Thus, providing the right hand side is non-negative the solution is non-negative. Observing that $\dfrac{d\Theta_i^0}{dh}=0$ if $\Theta^\infty(t_j)\geq\Theta_i^j(t)$ by induction it is possible to prove that $\dfrac{d\Theta_i^j}{dh}\geq 0$. As for the single layer slab the following function is defined

$$g(h)=\sum_{i=0}^{m}\left(\Theta^s(t_i)-\Theta_0^i\right)\delta t_i$$

and h is chosen as the value for which $g(h)=0$. From $\dfrac{d\Theta_i^j}{dh}\geq 0$ it is easy to prove that $g(h)$ is a monotone decreasing function so that a unique h which satisfy $g(h)=0$ can be found for example by the secant scheme.

7.4 *Choice of the mesh and experiment design*

Consider the heat equation for a single layer where physical parameters are independent on the temperature:

$$\frac{\partial}{\partial t}\Theta(t,z)=\frac{\kappa}{\rho c}\frac{\partial^2}{\partial z^2}\Theta(t,z)$$

the numerical scheme previously introduced is 1^0 order in time and 2^0 order in space i.e. it has an error of the form:

$$E_S\Delta t+E_M\Delta z^2 \tag{61}$$

where $\Delta t = 1/f_s$ being f_s the sampling frequency and Δz is the maximum size of the Finite Elements cells. From (61) the total error depends on two different contributions:

- An error due to the sampling frequency f_s; here referred as sampling error $S_E = E_S \Delta t$;
- An error due to the spatial discretization Δz; here referred as mesh error $M_E = E_M \Delta z^2$;

Consider the parameter

$$\mathcal{A} = \frac{E_S}{E_M} \frac{\Delta t}{\Delta z^2}$$

when $\mathcal{A} \gg 1$ it means that the error is dominated by the low sampling rate or by an excessive fine mesh. When $\mathcal{A} \ll 1$ it means that the error is dominated by the coarse mesh or by an excessive sampling rate. The parameter $\mathcal{A}$ can be used to optimize the mesh definition respect to the sampling frequency.

Normally the sampling rate is somehow determined by the hardware, so that from (61) the sampling error S_E bounds the maximum achievable accuracy.

The mesh definition is normally chosen in order to introduce a mesh error M_E of the same order of the sampling error S_E. However the sampling error is, in many practical applications, lower than the error introduced by parameter uncertainty (i.e. the values of the physical properties of the substrate given from the manufacturer, temperature measurement and so on). From the point of view of the experiment designer it is evident that mesh can be coarsened according to such an inaccuracy level.

It is worth to analyze the behavior of the error (61) as the sampling rate goes to ∞ and the parameter $\mathcal{A}$ is fixed. From this hypothesis and (61) the error becomes

$$\frac{E_S}{f_s} \left(1 + \frac{1}{\mathcal{A}}\right)$$

and

$$\Delta z = \left(\frac{E_S}{E_M}\frac{1}{f_s}\right)^{1/2},$$

The cost of each advancing step is proportional the mesh size which is in turn proportional to $1/\Delta z$; being the total number of steps proportional to $1/f_s$ the total cost is proportional to $f_s^{3/2}$ while the accuracy from (61) is proportional to $1/f_s$.

Because the total number of samples $n_s \propto f_s$ the computational cost is $\mathcal{O}\left\{n_s^{3/2}\right\}$ and accuracy is $\mathcal{O}\left\{1/n_s^2\right\}$ so that although the computational cost is apparently asintotically high the cost versus accuracy is not so bad.

However we observe that the computational effort is extremely low also in real test cases where $n_s \propto 10^4$ and for them the running time on a small PC is a few tens of seconds.

Moreover the finite elements approach permits to treat easily also the nonlinear cases when the temperature dependence of the physical properties cannot be neglected. Such an extension is not straightforward for methods based on transformations.

8 Numerical Results

8.1 Code validation

In order to validate the presented approach an ideal signal has been used having a know solution in the case of a semi-infinite slab with constant physical properties. This signal has been derived from the following expression of the impinging heat flux (George et al.; 1991)

$$\dot{q}_s(t) = \begin{cases} 0 & \text{for } t < 0 \\ A + B\cos 2\pi f_q t + \phi & \text{for } t \geq 0 \end{cases} \tag{62}$$

where A is the step magnitude, B is the superimposed signal magnitude, f_q is the frequency on the superimposed signal and ϕ is the phase of the superimposed signal. The surface temperature history which generates such an heat flux is

$$\begin{aligned} \pi^{1/2}\ (\rho c \kappa)^{1/2}\ \Theta^s(t) = 2At^{1/2} & + \frac{B}{f_q^{1/2}} \cos 2\pi f_q t + \phi \mathrm{F}_c \left(2\left(f_q t\right)^{1/2}\right) \\ & + \frac{B}{f_q^{1/2}} \sin 2\pi f_q t + \phi \mathrm{F}_s \left(2\left(f_q t\right)^{1/2}\right) \end{aligned} \tag{63}$$

and is valid with the above mentioned assumptions. Heat flux has been reconstructed from temperature signal (63) using the two formulations of the Cook and Felderman methods (implicit and standard one) and the finite elements code with various signal frequency f_0 and different sampling rates f_s. Both single and double layers configurations have been tested according to the approaches of sections 5–6–7. The test cases are listed in Table 1 Cases form 1 to 6 are related to the single layer thin film having macor® as substrate. The thickness of the layer was $5\,mm$ and the test duration was $1s$. Figure 4 shows the solution of test cases 1, 2 and 3 when temperature signal given in (63) is applied. Step like temperature signal is produced in the flow stream. Results are presented in terms of non dimensional heat flux (ratio of actual heat flux Q by the expected heat flux A) and non dimensional time scale ($t \cdot f_s$) for the three test cases. After a short initial time all methods give an excellent reconstruction. Implicit Cook and Felderman response seems to reconstruct the heat Heaveside signal better than Finite Elements and standard Cook and Felderman. Initial peak is suppressed. Notice that in the initial part of the signal (step region) Finite Element code reconstructs better than standard Cook and Felderman but worse than implicit Cook and Felderman. As higher the sampling frequency as faster the heat flux traces approach the actual value.

For a given accuracy requirement the size of the Finite Element mesh results fixed according to the considerations of section 7.4. The computational effort grows therefore linearly with frequency, while the better implementation of Cook and Felderman has an higher grow rate. Thus Finite Elements results to be cheaper than Cook and Felderman when data reduction of large data set is performed.

Table 1

single layer

test	$A[W/m^2]$	$B[W/m^2]$	$f_q[Hz]$	$f_s[Hz]$
1	1000	0	0	10
2	1000	0	0	100
3	1000	0	0	1000
4	1000	500	4	10
5	1000	500	4	100
6	1000	500	4	1000

double layer

test	$A[W/m^2]$	$B[W/m^2]$	$f_q[Hz]$	$f_s[Hz]$
7	1000	0	0	10
8	1000	0	0	100
9	1000	0	0	1000
10	1000	500	4	10
11	1000	500	4	100
12	1000	500	4	1000

In Figure 5 (test cases 4, 5 and 6 of Table 1), solution of (63) is given respectively for $f_s/f_q = 2.5$, 25, 50 and $B/A = 0.5$. The highest over estimation of the heat flux is due, analogously to the first 3 presented cases to standard Cook and Felderman. Signal reconstruction is poor for $f_s/f_0 = 2.5$ for all methods. The step is perfectly get from implicit method. Higher the ratio f_s/f_0, better is the reconstruction of oscillating part of the signal, however already at $f_s/f_0 = 25$ the reconstruction is very good in maximum amplitude and phase. Therefore only the first part of test 6 is depicted in figure 5c in order to show the signal reconstruction just during the initial step.

In order to validate the code in the case of double layer feature, the Finite Elements discretization has been used to compute $\Theta^s(t)$ from (62). $\dot{q}_s(t)$ has been afterwards reevaluated with finite elements and Cook and Felderman methods.

Step like heat functions results (test cases 7, 8 and 9 of table 1) are given in Figure 6. A value of

$$\frac{(\rho_1 c_1 \kappa_1)^{1/2}}{(\rho_2 c_2 \kappa_2)^{1/2}} \approx 0.04$$

and (see Figure 2)

$$\frac{a}{b-a} \approx 10^4$$

for the layers thickness ratio have been adopted. Maximum test duration was $1\ s$. Standard Cook and Felderman overestimates the actual heat flux. The absence of peek in the Finite Elements solution is essentially due to the procedure used to obtain the testing signals. On the same frequency base, longer times are necessary to approach the expected value of the heat flux compared to single layer cases. Oscillating test cases are depicted in Figures 7. Excellent reconstruction is performed for f_0/f_s ratio bigger than 25. Computational costs saves results to be even more evident than single layer case when Finite Elements code is adopted.

8.2 Experimental heat flux data reduction

The Finite Elements solution technique was finally used to processes rough data obtained from experimental facilities tests. In order to assess the performance for signals having different characteristic, four surface temperature histories have been selected. The test cases are listed in Table 2. Figure 8 show a typical tempera-

test	Facility – Location
13	Low Speed Tunnel – Trento University, Italy
14	CT2 Light Piston Isentropic Compression Tube – VKI, Belgium
15	H3 Mach 6 wind tunnel – VKI, Belgium
16	H3 wind tunnel – VKI, Belgium

Table 2

ture signal obtained in the short duration low speed tunnel (Mach < 0.1) of the turbomachinery lab of the University of Trento. upilex® layer of $75\,\mu m$ was used bounded on a plexiglass® wall of $15\,mm$ thickness as supporting substrate. The film was placed on the midpoint of the floor between two consecutive ribs. Further details are given in Battisti and Schmeer (1997). The sampling frequency was 500Hz. Because of the very noisy temperature signal, high scatter appears in heat flux reduction trace either in Finite Elements and both Cook and Felderman methods. Due to the summation in equation (27) and (31) these methods takes by for the longest CPU time for large n_s.

The second investigated signal is taken from measurements performed in the Light Piston Isentropic Compression Tube facility (CT2) at the von Karman Institute. Details of the experimental rig and the sensor are given in Pelle and Arts (1997). The temperature signal belongs to a single layer thin film (platinum over macor®) placed well down stream of the tripping wire of a flat plate. The sensor was subjected to a 0.7 Mach short duration flow stream. The surface temperature history is depicted in Figure 9a. The three processing methods are reported in Figure 9b-d. A good agreement results from their comparison.

The third test case was a compression ramp in the H3 Mach 6 wind tunnel of the von Karman Institute. Single layer thin film (platinum over macor®) was used. Figure 10a shows the temperature evolution of the upper and lower faces of a machined macor® model. Data were sampled at 250Hz. The model was injected in the MAch 6 flow having a free stream temperature of about $520K$. Further details are given in Marquet and Charbonnier (1998a-b). Right side Figure 10b shows the result obtained with Finite Element code. Similar solution method was used at the von Karman Institute for data reduction and the two solution (here not reported for seek of brevity) does not show any consistent difference. The lower pictures 10c-d show respectively the same temperature signal and the corresponding heat flux solution but performed when a sampling rate of 25Hz instead of the original 250Hz are used. A part of the inherent noise filtration effect, the Finite Element code seems to perform (as expected from the previous validation results) an accurate heat flux reconstruction.

When model back surface temperature significantly changes during the test, semi-infinite assumption is not longer valid and the Cook and Felderman like techniques cannot be safely used. Moreover if the model body even experiences significant temperature rise, constant physical properties assumption can introduce further errors in the solution. If the latter is the case either analog and Cook and Felderman methods are not accurate and numerical discretization are forced. In Figure 11a a typical example is presented. Temperature histories of the upper and lower surface of the same model of test case 15 measured by means of single layer thin films (platinum over macor®). The model was first heated up to $550K$ by infrared lamps, successively the lamps were switched off and the model was injected in vacuum. Figure 11b shows the corresponding heat flux signal obtained by using the Finite Elements code implemented with constant physical properties. Absolute differences are less then 10^{-3} respect to the solution obtained at the von Karman Institute. When temperature variable properties are considered, a small difference between the two solution becomes evident and results in a sligtly overestimation of the heat flux during the heating phase and under estimation during the cooling one (as shown in Figure 11c). The maximum is of about 2.5% when an heat flux of about $200000\,W/m^2$ impinges.

9 Conclusions

Common data reduction procedure heat transfer measurement in short duration facility by means of single and double layer thin film, have been reviewed and discussed. A simple Finite Elements discretization has been implemented and its ability to accurately reconstruct signals of known testing functions (as Heaveside signal with superimposed fluctuations) has been checked. Experimental not filtered data of various sampling frequency and flow characteristic have been processed. The implementation of temperature variable physical properties of the body has been discussed for a typical test case when its influence on accuracy cannot be neglected. Results seem to confirm the very good performance of the code which shows a very accurate signal reconstruction also at very low sampling frequencies. When semi-infinite slab assumption is not longer the case (i.e. leading edge of blades) numerical discretization such as Finite Elements approach is not negotiable. Further improvement of the code will be the development of a 2-D scheme in order to consider problems where lateral conduction effect cannot be neglected, and the evaluation of the influence of heat flux generated by Joule effect into the sensor.

10 Acknowledgment

We thankfull acknowledge professor T.Arts and professor J.M.Charbonnier of the von Karman Institute for useful discussions and for providing us the experimental data.

References

[1] R. W. Ainsworth, J. L. Allen, M. R. D. Davies, and J. E. D. et al., *Developments in instrumentation and processing for transient heat transfer measurement in a full stage model turbine*, Transaction of ASME, **111** (1989) 20–27.

[2] O. Axelsson, **Iterative Solution Methods** (Cambridge University Press, 1994).

[3] L. Battisti and T. Arts, *Wall heat transfer measurements in rib-roughened cooling channels by means of a transient technique*, ATI 51^0 Convegno ATI, Udine 16–20 Settembre (1996) 811–822.

[4] L. Battisti and T. Schmeer, *Experimental study of the surface heat transfer enhancement in a rib roughened blade coolant channel by means of double layer thin films*, Proceedings of the 55^o Eurotherm Seminar, Santorini, Greece.

[5] E. Bertolazzi, *Numerical conservation and discrete maximum principle for elliptic pdes*, Mathematical Models and Methods in Applied Sciences, **8** (1998) 685–711.

[6] C. Camci and T. Arts, *Experimental heat transfer investigation around the film cooled leading edge of a high pressure gas turbine rotor blade*, ASME Paper n. 85-GT-114 Houston Texas.

[7] H. Consigny and B. E. Richard, *Short duration measurement of heat transfer rate to a gas turbine rotor blade*, Journal of Engineering for Power, **104** (1982) 542–551.

[8] W. J. Cook and E. J. Felderman, *Reduction of data from thin film heat transfer gauges: A concise numerical technique*, AIAA Journal, **4** (1966) 561–562.

[9] T. E. Diller, **Advances in Heat Transfer Vol 23** (Academic Press, 1991).

[10] J. E. Doorly, *Procedures to determining surface heat flux using thin film gauges on a coated metal model in a transient test facility*, ASME, 87-GT-95.

[11] J. E. Doorly and M. L. G. Oldfield, *The theory of advanced multi-layer thin film heat transfer gauges*, Int. J.Heat Mass Transfer, **30** (1987) 1159–1168.

[12] M. G. Dunn, *Phase and time resolved measurement of unsteady heat transfer and pressure in a full-stage rotating turbine*, ASMEe Paper n. 89-GT-135.

[13] M. G. Dunn and A. Hause, *Measurement of the heat flux and pressure in a turbine stage*, ASME Journal of Engineering for Power, **104** (1981) 215–223.

[14] M. G. Dunn, H. L. Martin, and M. J. Stanek, *Heat flux and pressure measurement and comparison with prediction for a low aspect ratio turbine stage*, ASME Journal of Turbomachinery, **108** (1986) 108–115.

[15] W. K. George, W. J. Rae, and S. H. Woodward, *An evaluation of the analog and numerical techniques for unsteady heat transfer measurement with thin film gauges in transient facilities*, Experimental Thermal and Fluid Science, **4** (1991) 332–342.

[16] S. M. Guo, M. C. Spencer, G. D. Lock, and T. V. Jones, *The application of thin film gauges on flexible plastic substrate to the gas turbine situation*, Paper offered for 1995 ASME Turbo Expo, Huston, USA.

[17] J. Lukasiewicz, **Experimental Methods in Hypersonic** (Marcel Dekker, 1973).

[18] B. Marquet and J. M. Charbonnier, *Shock wave boundary layer interaction on hot surfaces: Analisys of the results of the thest campaign for the study of wall temperature effects*, Technical Note GSTP1-TR-6501-VKIN.

[19] B. Marquet and J. M. Charbonnier, *Shock wave boundary layer interaction on hot surfaces: Pressure and heat transfer measurements on hot wall compression ramp models at mach 6*, Technical Note GSTP1-TR-6301-VKIN.

[20] R. F. Meyer, *A heat flux meter for use with thin film surface thermometers*, NRC Canada, Aero Rep. LR279.

[21] M. L. G. Oldfield, T. V. Jones, and D. L. Schultz, *On-line computer for transient turbine cascade instruments*, IEEE Transactions on Aerospace and Electronic Systems AES-14, **5**.

[22] O. Pelle and T. Arts, *Development of a double layer thin film gauge for surface heat transfer measurement*, Proceedings of the 55^0 Eurotherm Seminar, Santorini, Greece.

[23] A. Pope and K. L. Goin, **High Speed Wind Tunnel Testing** (Wiley and Sons, 1965).

[24] D. L. Schultz and T. V. Jones, *Heat transfer in short duration hypersonic facilities*, AGARD AG 165.

[25] C. W. Shu and S. Osher, *Efficient implementation of essentially non-oscillatory shock-capturing schemes*, J. Comput. Phys., **77** (1988) 439–471.

[26] J. Stoer and R. Bulirsch, **Introduction to Numerical Analysis** (Springer, 1993).

[27] J. P. Vermeulen and G. Simeonides, *Parametric studies of shock wave /boundary layer interactions over 2-d compression corners at mach 6*, VKI Technical Note 181.

[28] R. J. Vidal, *Model instrumentation technique for heat transfer and force measurements in a hypersonic shock tunnel*, C.A.L. report AD-917-A-1.

[29] O. C. Zienkiewicz and R. L. Taylor, **The Finite Element Method** (Mc Graw Hill, 1989).

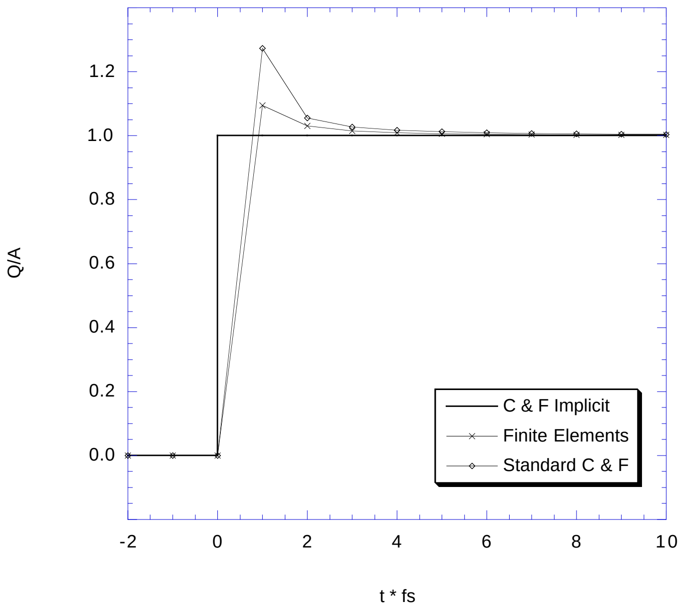

Fig. 4. Single layer heat flux reconstruction (tests 1, 2, 3)

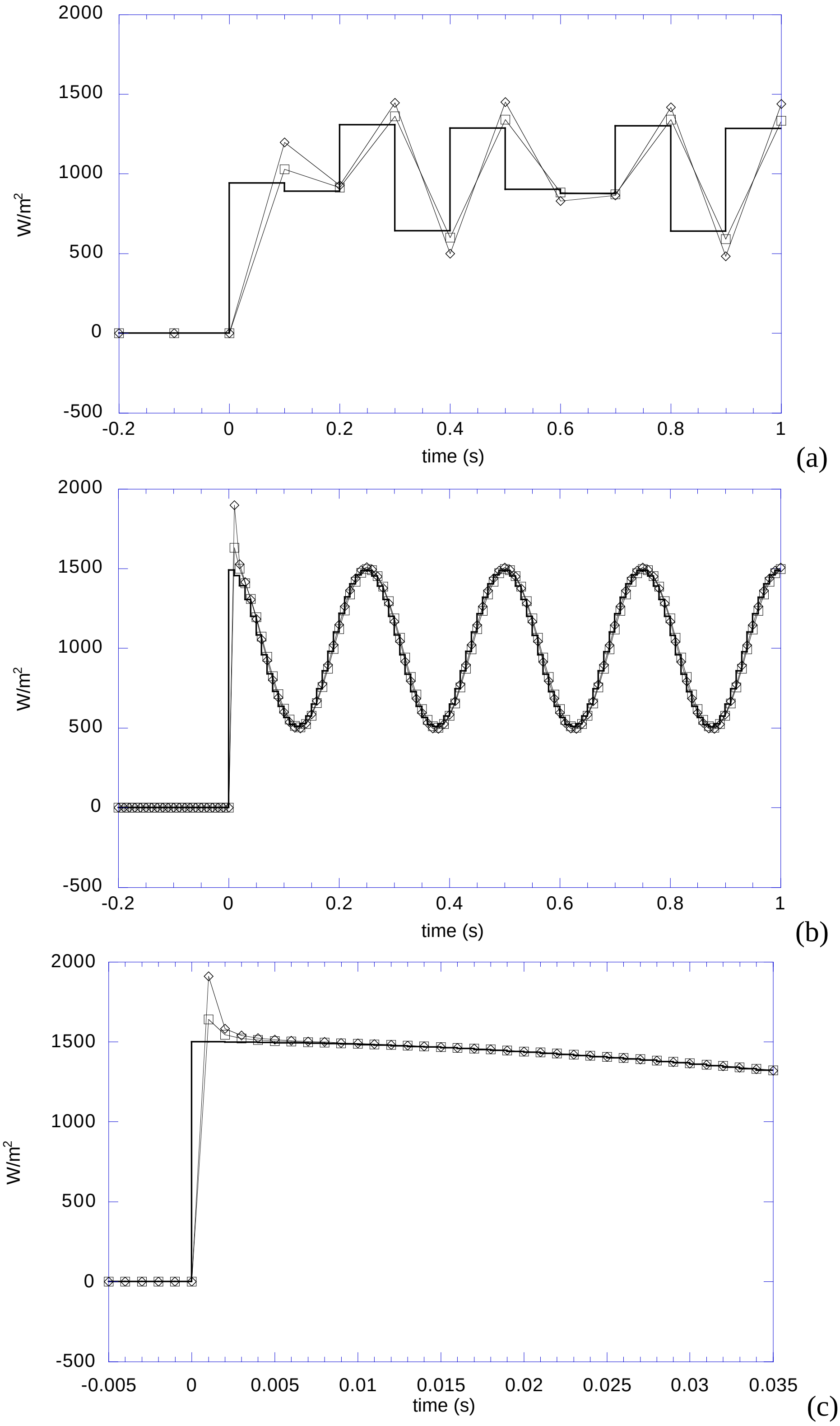

Fig. 5. Oscillating signal reconstruction for single layer configuration (tests 4, 5, 6)

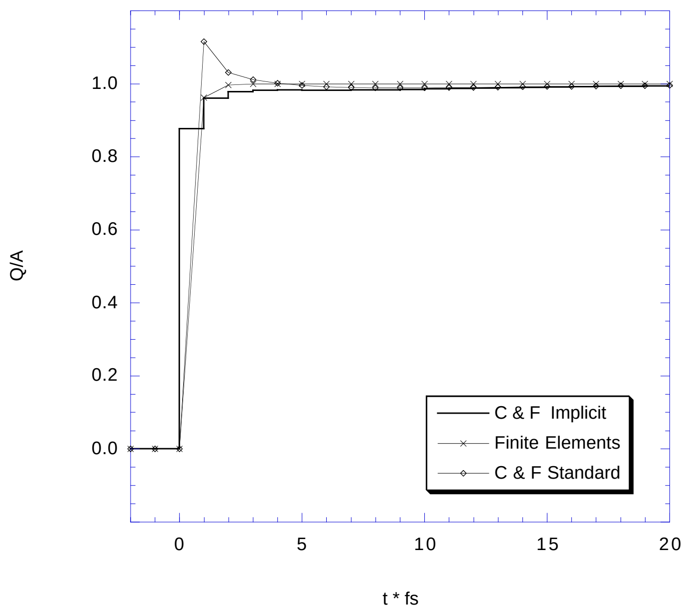

Fig. 6. Double layer heat flux reconstruction (tests 1, 2, 3)

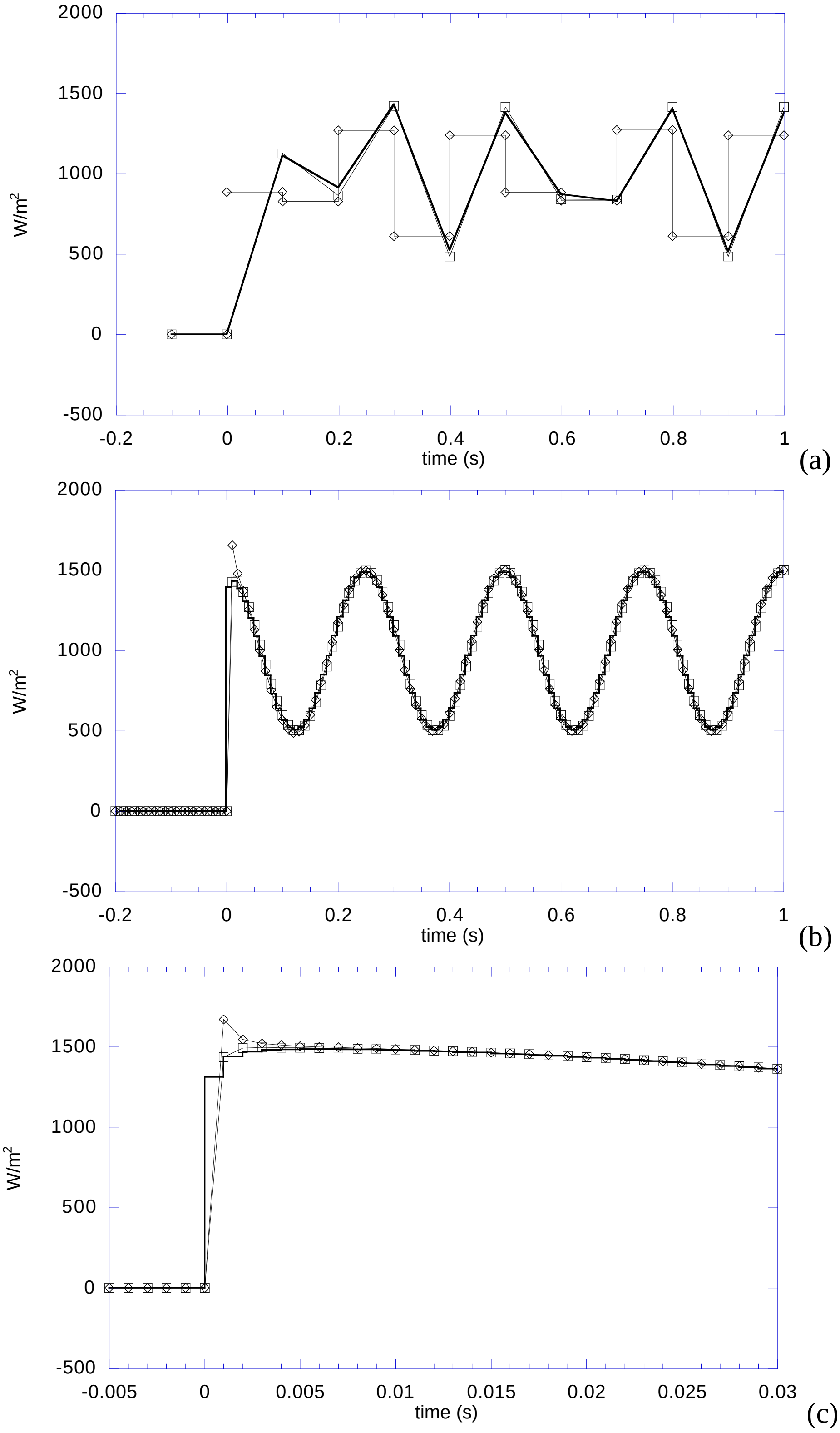

Fig. 7. Oscillating signal reconstruction for double layer configuration (tests 10, 11, 12)

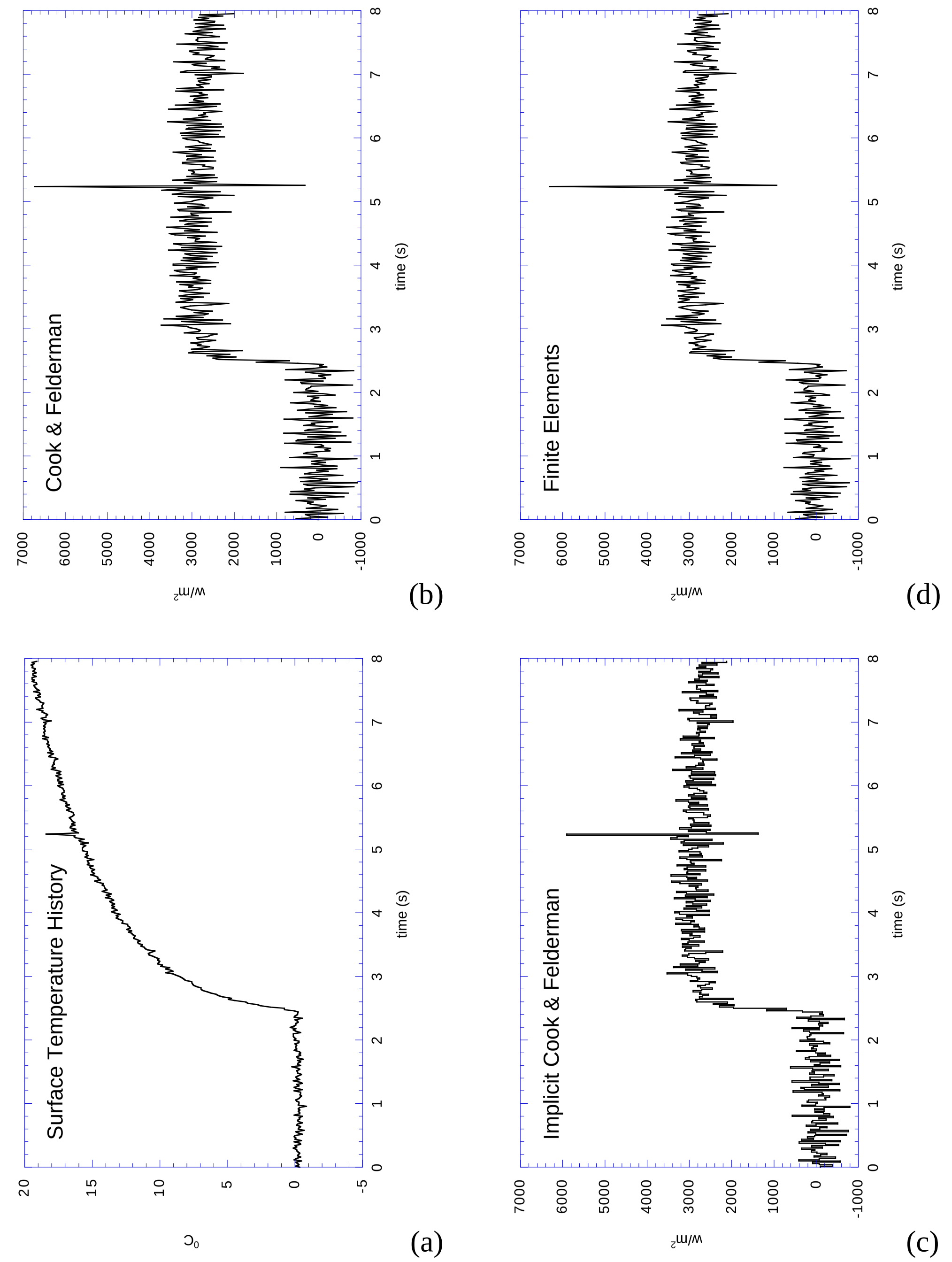

Fig. 8. Double layer thin film surface temperature signal and heat flux computation for test case 13

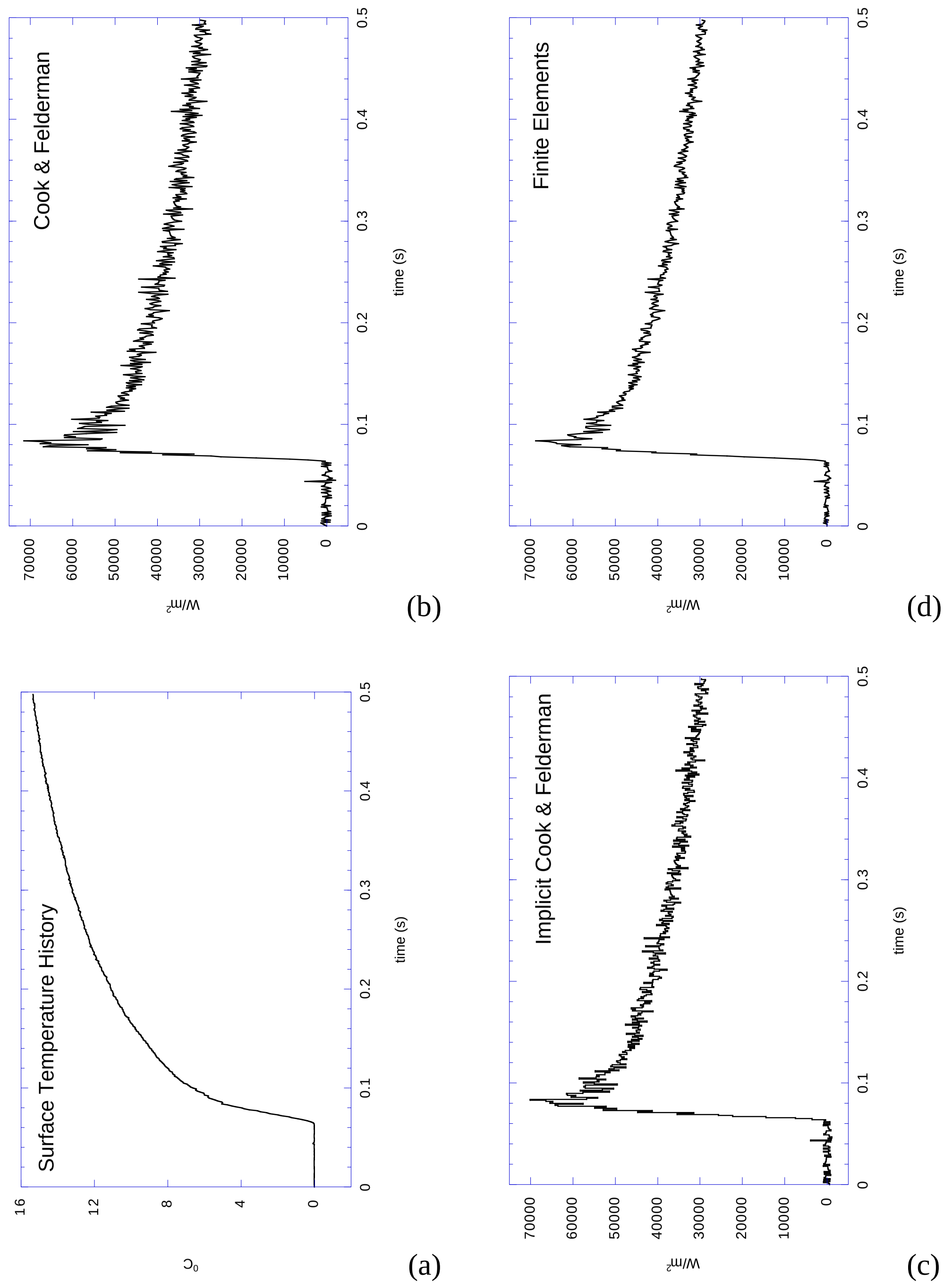

Fig. 9. Single layer thin film surface temperature signal and heat flux computation for test case 14 at Mach 0.7

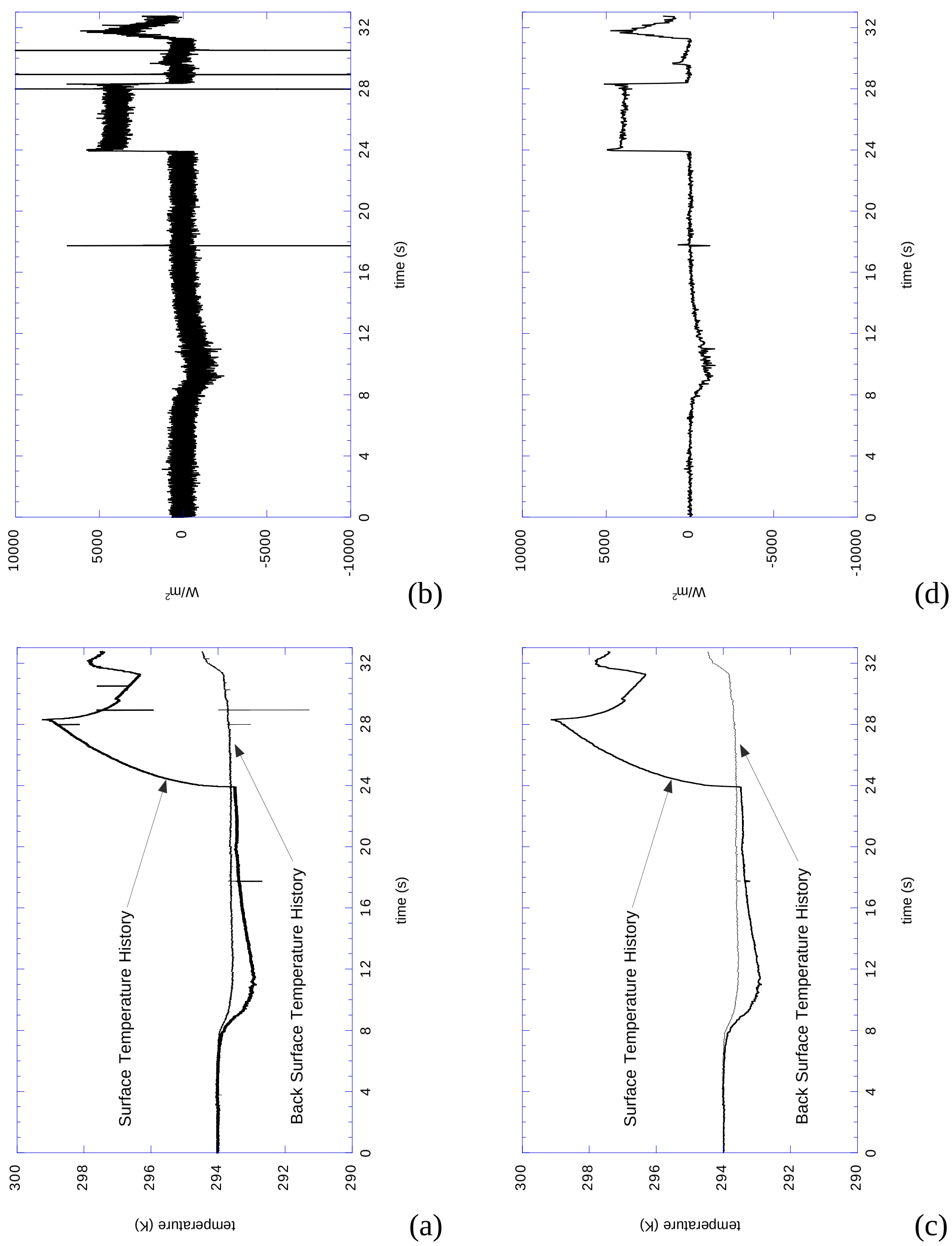

Fig. 10. Single layer thin film surface temperature signal and heat flux computation for test case 15

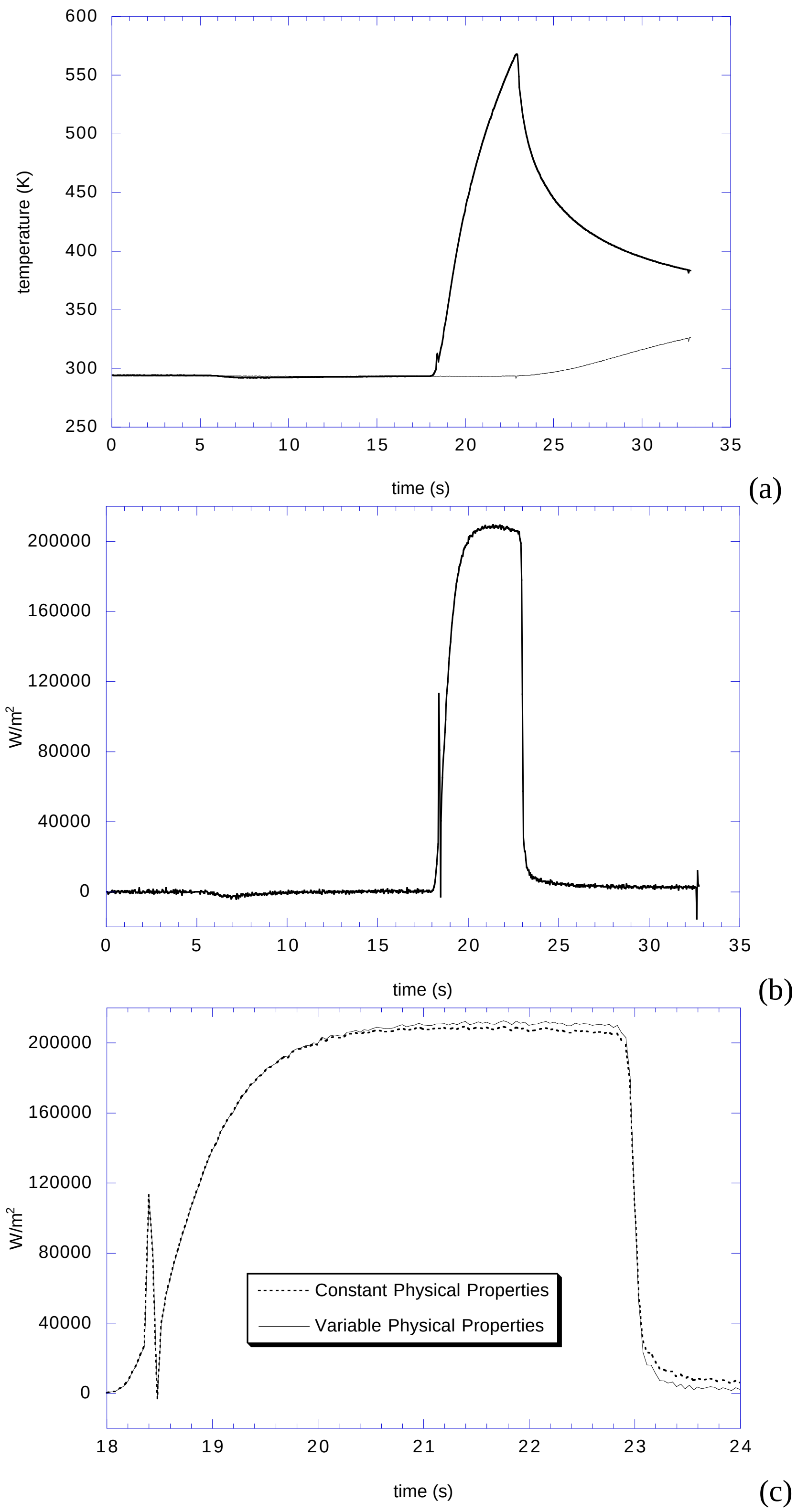

Fig. 11. Single layer thin film surface temperature signal and heat flux computation for test case 16